

Partial covering of emission regions of Q 0528–250 by intervening H₂ clouds.

V.V. Klimenko^{1,2}, S.A. Balashev^{1,2}, A.V. Ivanchik^{1,2}, C. Ledoux⁴,
 P. Noterdaeme³, P. Petitjean³, R. Srianand⁵, D.A. Varshalovich^{1,2}

¹ Ioffe Physical-Technical Institute of RAS, Polytekhnicheskaya 26, 194021 Saint-Petersburg, Russia

² St.-Petersburg State Polytechnical University, Polytekhnicheskaya 29, 195251 Saint-Petersburg, Russia

³ Université Pierre et Marie-Curie, Institut d’Astrophysique de Paris, CNRS-UMR7095, 98bis boulevard Arago, 75014 Paris, France

⁴ European Southern Observatory, Alonso de Córdova 3107, Casilla 19001, Vitacura, Santiago 19, Chile

⁵ Inter-University Centre for Astronomy and Astrophysics, Post Bag 4, Ganesh Khind, Pune 411 007, India

Accepted 15.12.2014 Received 08.10.2014

ABSTRACT

We present an analysis of the molecular hydrogen absorption system at $z_{abs} = 2.811$ in the spectrum of the blazar Q 0528–250. We demonstrate that the molecular cloud does not cover the background source completely. The partial coverage reveals itself as a residual flux in the bottom of saturated H₂ absorption lines. This amounts to about $(2.22 \pm 0.54)\%$ of the continuum and does not depend on the wavelength. This value is small and it explains why this effect has not been detected in previous studies of this quasar spectrum. However, it is robustly detected and significantly higher than the zero flux level in the bottom of saturated lines of the Ly α forest, (-0.21 ± 0.22) per cent. The presence of the residual flux could be caused by unresolved quasar multicomponents, by light scattered by dust, and/or by jet-cloud interaction. The H₂ absorption system is very well described by a two-component model without inclusion of additional components when we take partial coverage into account. The derived total column densities in the H₂ absorption components A and B are $\log N(\text{H}_2)[\text{cm}^{-2}] = 18.10 \pm 0.02$ and 17.82 ± 0.02 , respectively. HD molecules are present only in component B. Given the column density, $\log N(\text{HD}) = 13.33 \pm 0.02$, we find $N(\text{HD})/2N(\text{H}_2) = (1.48 \pm 0.10) \times 10^{-5}$, significantly lower than previous estimations. We argue that it is crucial to take into account the partial coverage effects in any analysis of H₂ bearing absorption systems, in particular when studying the physical state of high-redshift interstellar medium.

Key words: cosmology:observations, ISM:clouds, quasar:individual:Q 0528–250

1 INTRODUCTION

As a result of their cosmological distances quasars (QSOs) appear as point-like objects. Various studies have aimed to explore the detailed inner structure of quasars, which is unresolved even for low-redshift active galactic nuclei (AGNs), because of their remote distances and sub-parsec scales of their emission regions. In the standard AGN paradigm the central region is divided into an accretion disk, a dusty-torus, a jet, a broad line region (BLR), and a narrow line region (NLR). Each of these regions contribute differently to the AGN emission spectrum.

Direct imaging of the spatial structure of AGNs is possible with current instruments mainly probing longer scales. To date, several interferometric studies of the central engine of the brightest AGNs (e.g. Jaffe et al. 2004; Tristram et al. 2014; López-Gonzaga et al. 2014) have revealed the existence of a hot, parsec-scale disk that is surrounded by warm dust extended in the polar direction. In the optical band the geometry of the emission line region is investigated by indirect methods. Reverberation mapping establishes the relationship between the size and the luminosity of the BLR and yields a typical BLR size of $R_{\text{BLR}} \sim 0.2$ pc (Kaspi et al. 2007; Chelouche & Daniel 2012) for high redshift luminous

quasars. Differential microlensing allows for a constraint on the accretion disk size $\lesssim 3 \times 10^{-3}$ pc (Blackburne et al. 2011; Jiménez-Vicente et al. 2012) and for an estimation of the size of the BLR ~ 0.1 pc (Sluse et al. 2011). The observations of gamma-ray emission constrain the size of a jet constituent to a few parsecs (Abdo et al. 2010).

Another estimate of the size of the AGN emitting regions comes from constraints derived from covering factor analysis of intervening H_2 bearing clouds which happen to cover the background source only partially. Analysis of the partial coverage of Q 1232+082 by a molecular hydrogen absorption cloud allowed Balashev et al. (2011) to estimate the size of the C IV BLR, $R_{\text{CIV}} \sim 0.16^{+0.08}_{-0.11}$ pc.

Molecular hydrogen absorption systems, a subset of damped Ly α systems (DLAs) and sub-damped Ly α systems (sub-DLAs), reveal diffuse and translucent interstellar clouds in high redshift intervening galaxies (Noterdaeme et al. 2008). An analysis of H_2 absorption systems allows for examining the physical conditions of diffuse clouds in distant galaxies (Srianand et al. 2005; Noterdaeme et al. 2007). It has been shown that the gas is a part of the cold neutral medium with comparatively low kinetic temperature ($T \sim 50 - 500$ K) and high densities ($n_{\text{H}} > 10 \text{ cm}^{-3}$), thus compact sizes ($l \lesssim 1$ pc). Comparison of 21 cm and H_2 absorptions suggests that the H_2 absorption originates from a compact gas that probably contains only a small fraction of HI measured along the line of sight (Srianand et al. 2012). These systems are important instruments for the analysis of several cosmological problems, as follows. (i) The discovery of HD/ H_2 clouds at high redshift (Varshalovich et al. 2001) provides an independent way to estimate the primordial deuterium abundance (D/H) and therefore the relative baryon density of the Universe Ω_b which is one of the key cosmological parameters (Balashev et al. 2010; Ivanchik et al. 2010). (ii) The comparison of H_2 wavelengths observed in QSO spectra with laboratory ones (just for this quasar Q 0528–250, Varshalovich & Levshakov (1993), Cowie & Songaila (1995), Potekhin et al. (1998), Ubachs & Reinhold (2004), King et al. (2011)) allows us to test the possible cosmological variation of the proton-to-electron mass ratio $\mu = m_p/m_e$. Because the de-composition of H_2 absorptions into several components is crucial for studies of the fundamental constant variability problem, we should pay attention to the partial coverage effect. It is known that taking into account the partial coverage effects, the physical model of the absorption system differs (see Balashev et al. 2011). (iii) The interpretation of the relative populations of C I fine-structure excitation levels and CO rotational levels (Srianand et al. 2000; Noterdaeme et al. 2011) allows us to measure the temperature $T_{\text{CMB}}(z)$ of the cosmic microwave background radiation at high redshift.

Here, we argue that it is necessary to take into account the partial coverage of quasar emission regions by a compact intervening H_2 cloud in order to derive a robust fit of the absorption lines. If this effect is not taken into account, column densities can be underestimated by a factor of up to two orders of magnitude. The first case of such an analysis has been presented by Balashev et al. 2011 for Q 1232+082. The second case of partial coverage has been detected by Albornoz Vásquez et al. (2014) for H_2 bearing cloud towards the quasar Q 0643–504. The third case of par-

tial coverage for the H_2 cloud at $z_{\text{abs}} = 2.811$ in the spectrum of Q 0528–2508 is presented in this study. We analyse a new spectrum and detect residual flux in the bottom of saturated H_2 lines ($J = 0$ and $J = 1$ levels). In case this flux is not taken into account, saturated lines yield large χ^2 values and a multicomponent model is used instead (e.g. King et al. 2011).

The remainder of this paper is organized as follows. A brief description of the data is given in Section 2. The principles of partial coverage are described in Section 3. In Section 4, we present the analysis of the H_2 absorption system, accounting for partial coverage. The HD molecular lines are explored in Section 5. The results are discussed in Section 6, and we give a brief conclusion in Section 7.

2 DATA

The molecular hydrogen was identified for the first time at high redshift in the very spectrum of Q 0528–2508 (Levshakov & Varshalovich 1985). This quasar was observed many times, in particular during the period between 2001 and 2009 using both spectroscopic arms of Ultraviolet and Visual Echelle Spectrograph (UVES) of the Very Large Telescope (VLT); for a description of the instrument, see Dekker et al. (2000). The log of the observations used in our work is shown in Table 1. These observations relate to four programmes, three of which were carried out in 2001–2002: 66.A-0594(A) (PI: Molaro), 68.A-0600(A) (PI: Ledoux), and 68.A-0106(A) (PI: Petitjean). The instrument settings used during these observations were a 1-arcsec slit and 2x2 CCD pixel binning in both arms, resulting in a resolving power of $R \sim 45000$ in the blue and $R \sim 43000$ in the red. There was no ThAr lamp calibration attached to each of the exposures. An additional series of observations was performed in 2008–2009 under programme 082.A-0087(A) (PI: Ubachs). The settings for that programme were a 0.8-arcsec slit in the blue arm and a 0.7-arcsec slit in the red. The 2x2 CCD pixel binning was also used at that time. This resulted in a resolving power of $R \sim 60000$ in the blue and $R \sim 56000$ in the red. Because the goal of that programme was to set a limit on the variation of μ , ThAr lamp calibrations were also taken immediately after each observation.

The data presented in Table 1 were reduced using the UVES Common Pipeline Library (CPL) data reduction pipeline release 4.9.5 using the optimal extraction method¹. The inter-order background (scattered light inside the instrument) was carefully subtracted in both the flat-field frames and the science exposures. Linear spline interpolation was used to produce a two-dimensional background image, which was subsequently smoothed using an average boxcar. Fourth-order polynomials were used to find the dispersion solutions. However, the errors only reflect the calibration error at the observed wavelengths of the ThAr lines used for wavelength calibration. All the spectra were corrected for the motion of the observatory around the barycentre of the Solar system and then converted to vacuum wavelengths. These spectra were interpolated into a common wavelength

¹ see the UVES pipeline user manual available for download at [ftp://ftp.eso.org/pub/dfs/pipelines/uves/uvess-pipeline-manual-22.8.pdf](http://ftp.eso.org/pub/dfs/pipelines/uves/uvess-pipeline-manual-22.8.pdf)

Table 1. Log of the observations

No.	UT Date	Program ID	Exposure (sec)	Slit (arcsec)
1	03.02.2001	66.A-0594(A)	1×5655	1.0
2	04.02.2001	66.A-0594(A)	2×5655	1.0
3	05.02.2001	66.A-0594(A)	1×5655	1.0
4	07.02.2001	66.A-0594(A)	1×5655	1.0
5	13.02.2001	66.A-0594(A)	1×5655	1.0
6	13.03.2001	66.A-0594(A)	1×5655	1.0
7	15.03.2001	66.A-0594(A)	1×5655	1.0
8	17.10.2001	68.A-0600(A)	1×3600	1.0
9	18.10.2001	68.A-0600(A)	2×3600	1.0
10	08.01.2002	68.A-0106(A)	2×3600	1.0
11	09.01.2002	68.A-0106(A)	2×3600	1.0
12	10.01.2002	68.A-0106(A)	2×3600	1.0
13	23.11.2008	082.A-0087(A)	2×2900	0.8–0.7
14	25.11.2008	082.A-0087(A)	1×2900	0.8–0.7
15	23.12.2008	082.A-0087(A)	4×2900	0.8–0.7
16	25.01.2009	082.A-0087(A)	1×2900	0.8–0.7
17	26.01.2009	082.A-0087(A)	1×2900	0.8–0.7
18	26.02.2009	082.A-0087(A)	1×2900	0.8–0.7
Total			108450	

array and generated the weighted-mean combined spectrum using the inverse squares of errors as weights. All the available exposures were utilized to increase the signal-to-noise ratio up to ~ 60 per pixel in the wavelength range of the H_2 absorption lines (at $z = 2.811$). As shown below, this allows us to detect and study the effect of partial coverage in details.

3 EFFECT OF PARTIAL COVERING

Partial covering implies that only a part of the background source is covered by the absorbing cloud. Mainly this can be a consequence of the absorbing cloud size being comparable to, or even smaller than, the projected extent of the background source.

Partial covering is readily detectable in the spectrum of a background quasar if the cores of the saturated absorption lines do not reach the zero flux level. This indicates that a part of the radiation from the QSO passes by the cloud. The covering factor characterizing partial coverage is defined by the ratio,

$$f_c = \frac{F_{\text{cloud}}}{F_{\text{total}}}, \quad (1)$$

where F_{cloud} is the flux that passes through the absorbing gas and F_{total} is the total flux. Therefore the measured flux in the spectrum, $F(\lambda)$, can be written as:

$$F(\lambda) = [F_{\text{total}}(\lambda) - F_{\text{cloud}}(\lambda)] + F_{\text{cloud}}(\lambda) \exp[-\tau(\lambda)], \quad (2)$$

here $\tau(\lambda)$ is the optical depth of the cloud at the wavelength λ . The line flux residual (LFR) is the fraction of the QSO flux which is not covered by the cloud. These definitions are

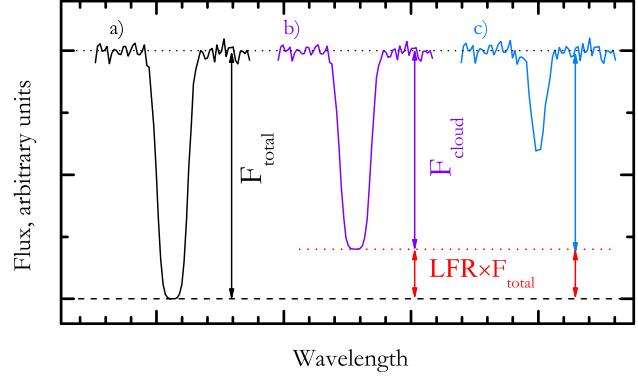


Figure 1. An illustration of the effect of partial coverage on the absorption-line profiles. Different panels show (a) a highly saturated line with total coverage, $f_c = 1$, (b) a highly saturated line with partial coverage, $f_c = 0.8$ and (c) a partially saturated line with the same partial coverage, $f_c = 0.8$. The line flux residual (LFR) is the fraction of the QSO flux that is not intercepted by the cloud. It can be easily derived from the spectral analysis in case (b), but it is not straightforward to detect in case (c).

illustrated in Fig. 1. The determination of the covering factor is trivial in the case of highly saturated absorption lines (see Fig. 1 panels (a) and (b)) while for a partially saturated line (see Fig. 1 case (c)) the analysis requires a more sophisticated procedure. In this case it is necessary to use several absorption lines originating from the same levels but with different values of λf , which is the product of the oscillator strength, f , and the wavelength of the transition, λ . Such an analysis has been performed by Ivanchik et al. (2010) and more precisely by Balashev et al. (2011) for the spectrum of Q 1232+082, and by Albornoz Vásquez et al. (2014) for the spectrum of Q 0643–504. A similar situation was observed for HE0001–2340. Jones et al. (2010) have considered the possibility of partial coverage of the BLR to explain the observed $Mg\,II$ equivalent widths. In contrast to the rare situations where partial covering occurs from intervening systems (see also Petitjean et al. 2000), partial covering is typical for absorption systems associated with quasars (e.g. Petitjean et al. 1994; Rupke et al. 2005; Hamann et al. 2010; Muzahid et al. 2013).

A failure to take into account the partial coverage effect in a spectroscopic analysis can lead to a significant underestimation of the column density of an absorber. The systematic bias (of column density) can exceed several orders of magnitude for saturated lines. As an example, consider an absorption line which consists of one component and has the high column density. The spectrum and the corresponding one-component model are shown in panel (a) of Fig. 2. In panels (b), (c), (d) and (e) the same line is presented, but part of radiation from background source (10% for clarity) passes by a cloud. If we take into account the LFR, then the line can be properly fitted by a one component model and we can recover the high input column density (with given accuracy) and measure the LFR value (panel (e) of Fig. 2). If the residual flux is not taken into account, then the one component model – Lorentzian (b) or Gaussian (c) profiles – is not adequate, the reason being that a one-component Voigt profile cannot describe the unsaturated bottom and far wings of the line simultaneously. Using additional com-

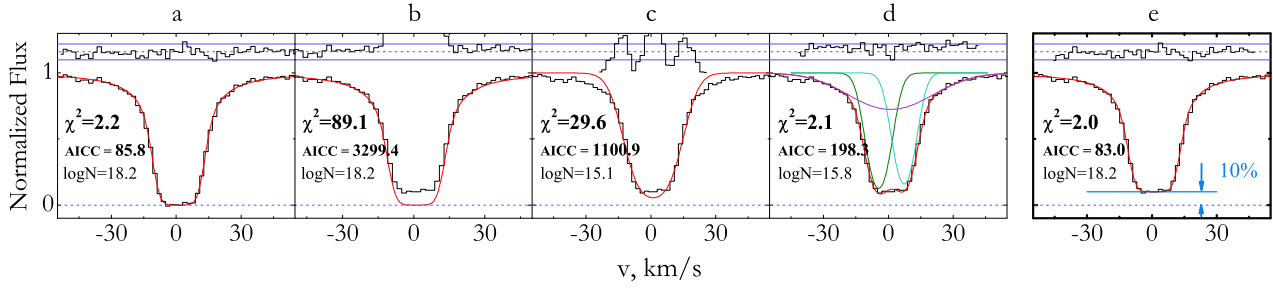


Figure 2. Panel (a) shows a single-component H_2 absorption line with $\log N = 18.2$ and $b = 4 \text{ km s}^{-1}$ and a fit by a one-component model (red line). The flux at the bottom of the line goes to zero. We add a residual flux of about 10 per cent (for clarity) to the data in panels (b), (c), (d) and (e). The flux at the bottom of the lines does not go to the zero level, and simultaneously the lines have Lorentzian wings. A simple one-component model cannot describe this line (cases (b) and (c)) and returns a large reduced χ^2 . However, if we add a new unresolved component to the model, the χ^2 will be significantly decreased (case (d)) but not the statistical criterion, the AICC (see King et al. 2011), and the returned column density will be two order of magnitude too small.

Table 2. Results of the previous analyses of the H_2 system at $z = 2.811$ towards Q 0528–250.

Year	$\log N_{\text{tot}}$	N _{Comp.}	Resolution	Ref.
1985	16.46 ± 0.07	1		[1]
1988	18.0	1	10 000	[2]
1998	16.77 ± 0.09	1	10 000	[3]
2005	$18.22^{+0.13}_{-0.17}$	2	40 000	[4]
2006	18.45 ± 0.02	–		[5]
2011	16.56 ± 0.02	3	45 000	[6]
2015	18.28 ± 0.02	2	45 000	This work

[1] Levshakov & Varshalovich (1985); [2] Foltz et al. (1988);
 [3] Srianand & Petitjean (1998); [4] Srianand et al. (2005);
 [5] Ćirković et al. (2006); [6] King et al. (2011)

ponents, as shown in panel (d), a result with a satisfactory χ^2 is obtained. However, this solution is incorrect, because the resulting column density ($\log N = 15.8$) is much smaller than the input one ($\log N = 18.2$). To distinguish between cases (d) and (e) we propose a new method based on an analysis of several absorption lines with different oscillator strengths. The description of the method and application to the analysis of H_2 in Q 0528–250 are described in more detail later.

4 MOLECULAR HYDROGEN

Molecular hydrogen lines are detected in the spectrum of Q 0528–250 from the DLA at $z_{\text{abs}} = 2.811$. Column density of neutral hydrogen in this DLA system is $\log N(\text{H}_1) = 21.35 \pm 0.07$ (Noterdaeme et al. 2008). H_2 lines correspond to transitions from rotational levels up to $J = 5$. To fit the molecular hydrogen lines, the spectrum has been normalized with a continuum constructed by fitting the selected continuum regions devoid of any absorptions with spline.

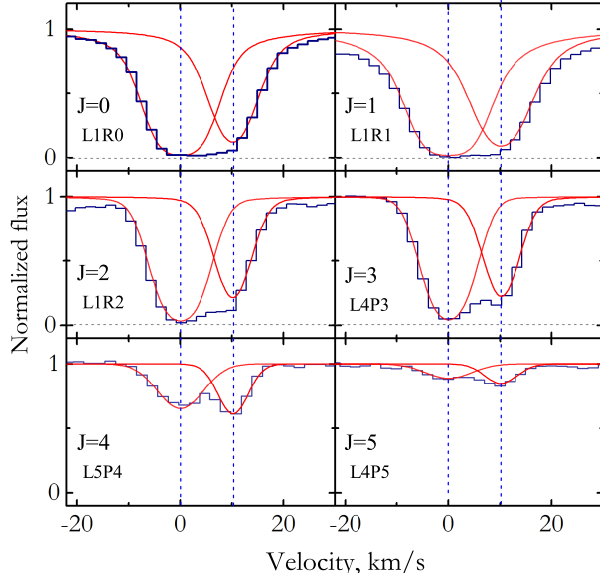


Figure 3. Examples of H_2 line profiles corresponding to the transitions from $J = 0 - 5$ levels. Two components are clearly seen in the $J = 4$ and 5 lines. We have found that two components are enough to obtain a satisfying χ^2 . The origin of the velocity scale is taken at the redshift of the H_2 component, $z_A = 2.8109$.

4.1 Number of components

The profiles of the H_2 absorption lines have a complex structure that cannot be fitted with a single component. At least two components are clearly seen in the lines corresponding to $J = 4, J = 5$ rotational levels (see Fig.3). Since the first identification of the H_2 system in the quasar (Levshakov & Varshalovich 1985) other studies have been conducted, providing discordant results (see Table 2). Srianand et al. (2005) used a two-component model, while King et al. (2011) pointed out that a three-component model is very strongly preferred over two-component model. King et al. (2011) used a fitting procedure where they increased the number of components in the absorption system in order to minimize the corrected Akaike information

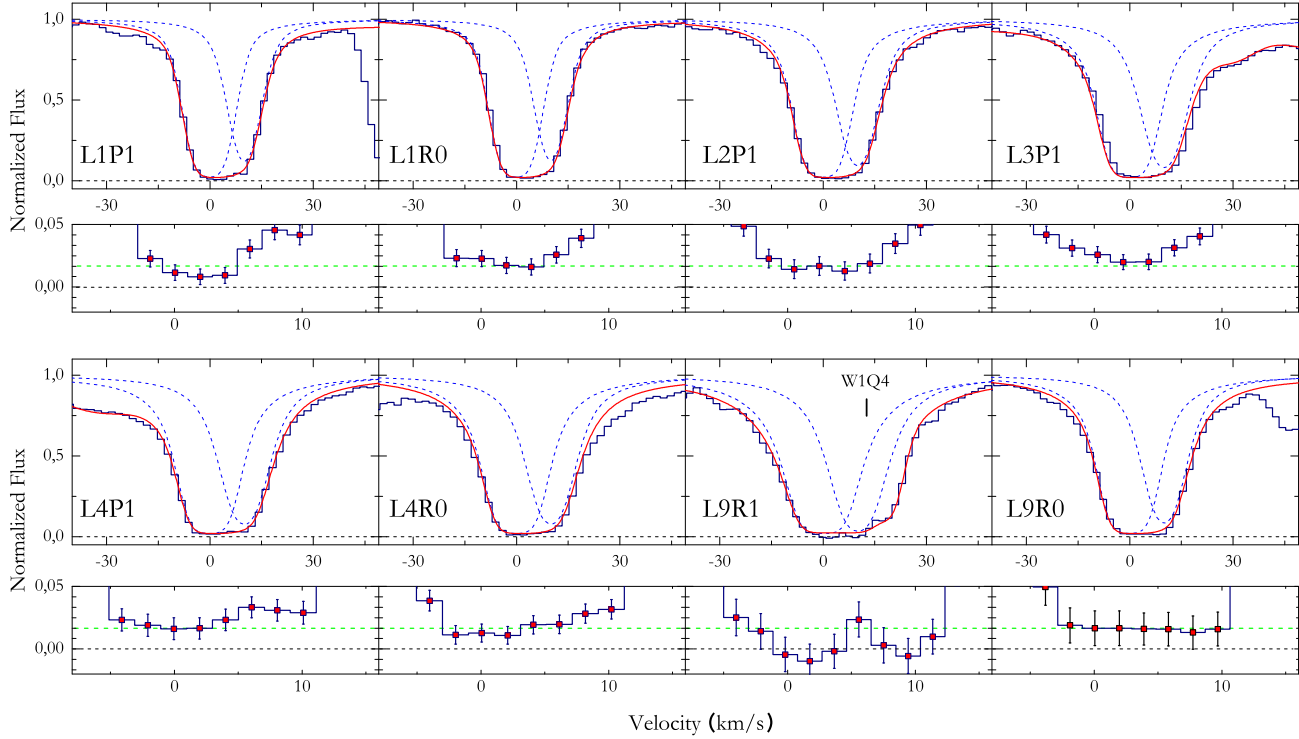


Figure 4. Some of the absorption lines of H_2 from the $J = 0, 1$ levels detected in the spectrum of Q 0528–250 and the best Voigt profile fit (red line). Two components of the absorption system are shown by blue dashed lines. Only unblended saturated lines are present. The presence of prominent Lorentzian wings of the lines indicate high H_2 column density. The additional panels show a close-up of the bottom of the corresponding lines. The dashed black horizontal line represents the zero flux level. It is clearly seen that about 2 per cent of the LFR is present at the bottom of the saturated H_2 lines. The x-axes show the velocity offset from the centre of H_2 component at $z = 2.81099$. In the profile of H_2 line L9R1, some pixels in the bottom of the line are lower than 2 per cent level, which is probably because this line is blended with Ly α forest absorption lines.

criterion, AICC² (Sugiura 1978; King et al. 2011). The resulting total column density differs by two order of magnitude from Srianand et al. (2005). In that case a criterion for choosing preferred model is the consistent derived physical parameters of a cloud. It can be noted note that by using H_2 column density reported by King et al. (2011) (based on the three-component model) a $N(\text{HD})/2N(H_2)$ ratio is obtained, that is about an order of magnitude higher than the primordial one. Meanwhile, the H_2 column density in two-component model of Srianand et al. (2005) gives a reasonable $N(\text{HD})/2N(H_2)$ ratio, which is consistent with the typical values measured at high redshift (Balashev et al. 2010).

A very important point for the choice of a reasonable absorption profile model in the case of Q 0528–250 is the presence of Lorentzian wings in $J = 0, J = 1$ line profiles (see Fig. 4). It is an indicator of the high H_2 column density of absorption system with $\log N(H_2) > 18$ which is consistent with the result reported by Srianand et al. (2005). However, in the new spectrum of Q 0528–250 the H_2 lines with prominent Lorentzian wings have some residual flux

² This statistical criteria allows for a choice of preferred model among several models with different numbers of fitting parameters. $\text{AICC} = \chi^2 + 2p + \frac{2p(p+1)}{n-p-1}$, where p is the number of fitting parameters, n is the number of spectral points, included in an analysis.

at the bottom which significantly differs from the zero flux level (see Fig. 4 and Fig. 5). As a consequence, the fit by Srianand et al. (2005) gives the large reduced χ^2 . It is probable that the signal-to-noise ratio in the previous spectrum was insufficient to detect the residual flux.

The current study shows that the residual flux detected in the bottom of saturated H_2 lines in the spectrum of Q 0528–250 is the result of a partial coverage effect. In this case, the profiles of H_2 lines can be very well fitted by two-component model. Therefore, there is no need to increase the number of components in H_2 profiles (such as it is done by King et al. 2011) to explain the complex structure of lines (an example is given in Fig. 2). In the next three subsections, we provide evidence of the existence of the partial coverage in the spectrum of Q 0528–250.

4.2 Zero-flux level correction

To measure the LFR in H_2 absorption lines we need to derive the zero flux level in the spectrum. A non-zero flux in the core of a saturated absorption line can be the result of inaccurate determination in between spectral orders of scattered light inside the instrument. The zero flux level in the spectrum can be estimated using the saturated Ly α absorption lines which are numerous and almost uniformly distributed over the wavelength range where H_2 absorption lines are lo-

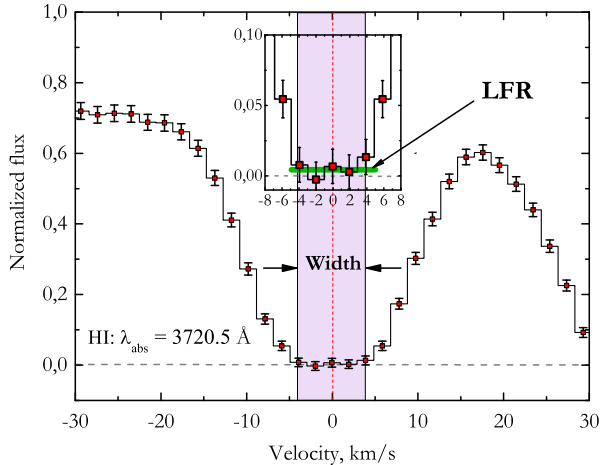


Figure 6. An illustration of the residual flux measurement procedure. To estimate the residual flux we determine the median flux for pixels in a line profile that are in the range of $\pm 1\sigma$ from the flux at the nearest pixel to the central wavelength λ_c . This region is shown by purple shading. We refer to the width of this region as the width of the bottom of the line.

cated. Ly α lines are associated with intergalactic clouds that are larger than several kpc, thus it is most likely that they cover the background source completely.

Wide flat bottom lines ($\Delta\lambda > 1 \text{ \AA}$, i.e. $\delta v > 80 \text{ km s}^{-1}$) were selected, which guarantees that lines are saturated and therefore measured fluxes in the bottom of the lines (LFRs) are the real zero flux level in the spectrum. These lines were selected in the spectral region $3500\text{--}4700 \text{ \AA}$. To estimate the residual flux at the bottom of the line the procedure illustrated in Fig. 6 was implemented. We selected several pixels in a line profile for which flux is within $f_c \pm 1\sigma_i$, where f_c is the flux at the centre of the line and σ_i is the error in pixel i . The residual flux was calculated as the median of the flux in the selected pixels. The width of the line bottom was estimated as the difference between the right most and left-most selected pixels from the line centre (see Fig. 6). The top-left panel of Fig. 5 shows the LFR values obtained for the selected saturated Ly α absorption lines. The average value is found to be $(-0.21 \pm 0.04)\%$. The standard deviation of the points is $\sigma \simeq 0.22\%$. The green stars show the LFR values measured at the bottom of the Ly α and Ly β lines associated with the DLA-system at $z_{\text{abs}} = 2.79$ and with the Ly α line of the second DLA-system at $z_{\text{abs}} = 2.14$. These lines are the most saturated lines for the spectrum.

4.3 Partial coverage of H₂ absorption lines

To estimate the residual flux in H₂ lines we selected J = 0, 1 lines without apparent blends. The LFR was measured by the same technique as for the Ly α forest lines. The analysis found that the flux in the bottom of the lines is quite constant over large velocity range $\delta v \simeq 10 \text{ km s}^{-1}$ (i.e. the dispersion of points is within the range of the average statistical error) that is wider than the full width half maximum (FWHM) of the UVES (6 km s⁻¹) and is comparable with the shift between centres of the two components. Therefore, the structure of H₂ system has no effect on the residual flux.

The comparison of the obtained residual flux in the J = 0, 1 H₂ lines with the level of the residual flux in the Ly α forest lines is shown in Fig. 5. The filled squares represent the residual flux in H₂ lines versus its location in the spectrum. We have estimated the line flux residual at the level $2.22 \pm 0.54\%$ of the continuum, which significantly exceeds the zero-flux level.

Non-zero residual flux at the bottom of saturated lines can also be the result of the convolution of the saturated lines with the instrumental function, or an imperfect data reduction, and/or of the blend of several unresolved unsaturated lines. First, however H₂ lines are wide with widths larger than the FWHM of the UVES spectrograph (6 km/s, i.e. $\sim 0.08 \text{ \AA}$), so after convolution with the instrument function, the flux at the bottom of these lines must still go to zero. Secondly, the improper data reduction is not a viable explanation of the residual fluxes of saturated Ly α lines are consistently equal to zero. Also we tested the dependence of residual flux on the width of the bottom of line for H₂ and for the Ly α forest lines. This is shown in Fig. B1. Several lines in the Ly α forest were detected; these have similar widths as the H₂ lines and go to the zero level. The profiles of these lines are shown in Fig. B2.

Lastly, the residual flux can not be a result of the composition of several unresolved unsaturated lines because the lines have Lorentzian wings.

4.3.1 The λf test

An additional test which confirms the presence of the partial coverage effect is discussed here (and illustrated in Fig. 7). Molecular hydrogen lines from J = 0, 1 levels have very different values of the product λf (from 0.6 for L0P1 to 36.0 for W1Q1). It is known that the flux in the bottom of an absorption line decreases exponentially when λf increases, $F \propto \exp(-\lambda f)$. The results of the calculation of this dependence for an absorption line in the spectrum with VLT resolution (FWHM = 6 km s⁻¹) are shown in Fig. 7 by the dashed lines. For simplicity, the modeled line profile consists of one component. The Doppler parameter $b = 4 \text{ km s}^{-1}$ and the Damping width Γ_{lm} is the same as for the H₂ line L2P1. Because the equivalent width of the line gets to the logarithmic part of the curve of growth, we do not consider the different Doppler parameters. Two dashed curves (violet and grey) are calculated for the line with column densities $\log N = 15$ and 16. The curve is shifted from right to left as the column density N increases. For a higher column density, the residual flux equals zero for a wide range of λf (because the line is saturated) and differs from zero only for small values of $\lambda f \leq 5$ (the case of an unsaturated line). In a case of a multicomponent line (i.e. the blend of two or three lines with small column density $\log N = 15$), the residual flux in the bottom of the blended line would also behave exponentially (dashed-dot curves). However, the behavior of the residual fluxes in the bottom of the saturated H₂ lines in the spectrum of Q0528-250 is quite different. The residual fluxes in the H₂ lines are shown by the filled blue and red squares. The squares do not follow the expected behavior, moreover the points scatter similarly around a median value in the whole range of λf .

Two models were applied to obtain a consistent and correct fit to the H₂ lines. Model (i) considers the best fit of

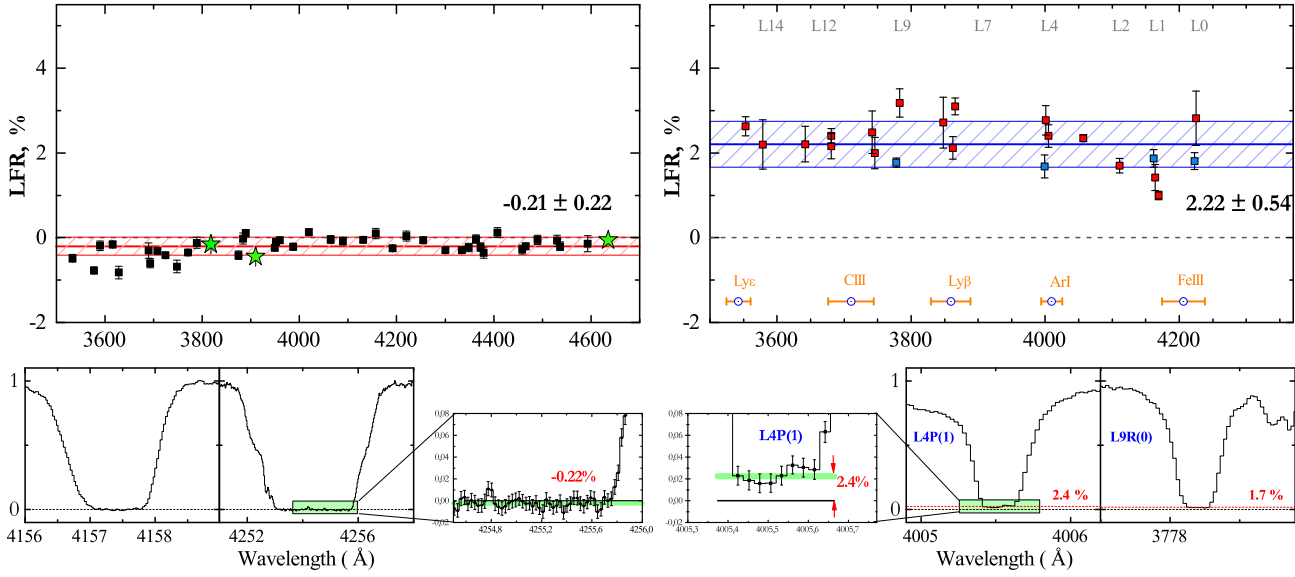


Figure 5. Top left: Analysis of the zero flux level in the spectrum of Q 0528–250. The LFRs measured at the bottom of the saturated absorption lines in the Ly α forest are plotted against the wavelength as filled squares. The residual fluxes are expressed in per cent of the continuum. The green stars show the LFR measured in the Ly β and Ly α absorption lines of the DLA system at $z_{\text{abs}} = 2.79$ and the Ly α absorption from the DLA system at $z_{\text{abs}} = 2.14$. The average value of the zero flux level is shown by the red horizontal line. The scatter in the LFR at the bottom of the lines (i.e. noise in the spectrum) is found to be at the level of 0.22 per cent. Bottom left: a few examples of saturated Ly α lines. The third bottom panel is the zoom of a part of the second panel. Top right: the residual fluxes at the bottom of the H $_2$ absorption lines from rotational levels $J = 0$ (blue) and $J = 1$ (red) are plotted against wavelengths as filled squares. The average value of the LFR in the H $_2$ lines is shown by the blue line. Blue circles and orange horizontal lines show the positions of QSO broad emission lines and their widths taken from Vanden Berk et al. (2001). Bottom right: A few saturated H $_2$ absorption lines are present. The red dashed lines show the estimated residual flux in each H $_2$ line. The black line indicates the zero level. The first panel shows the zoom of a part of the second panel. It can be seen that the flux in the pixels located at the bottom of saturated H $_2$ lines systematically departs from zero. The shift is about 2 per cent of the continuum.

the certain H $_2$ line (e.g. L2P1), which has a value of $\lambda f = 4.23$ and LFR = 1.7% of the total flux. The line has a wide flat bottom ($\delta v \sim 10 \text{ km s}^{-1}$) and Lorentzian wings. To fit this line without the partial coverage, it is necessary to use several unsaturated components in the line profile. Therefore, this model describes the line profile well. Model (ii) takes into account the partial coverage, and the line L2P1 can be fitted by the one-component model with high column density $\log N = 18.2$ and LFR = 1.7% (the blue line in the right-hand top panel). This model also describes the line profile accurately. Using only one H $_2$ line we cannot determine the most probable model. However, if we consider several H $_2$ lines from the same J level which cover a wide range of λf , we will be able to discriminate it. It is known that the lines from the same J level correspond to the same physical region of a molecular cloud; therefore the lines are described by the same set of physical parameters (the column density N and Doppler parameter b). The difference between line profiles originating from the same J level is caused only by the different values of λf for the lines. Therefore, the correct model of an absorption system must describe all measurements of residual flux in the bottom of lines from a given J level simultaneously. Using the best fit parameters for models (i) and (ii) we have calculated the dependence of the residual flux on λf (thick red and blue curves, respectively). The thick red line cannot describe all squares in the main panel simultaneously, whereas the blue thick line can.

4.4 Voigt profile Fitting

A Voigt profile fitting of the H $_2$ absorption lines was performed, taking into account the partial coverage. To describe a complex structure of line profiles we have divided the total flux detected by an observer into two parts: from a main source and an additional one. In addition, we consider the H $_2$ system to be composed of two components (A and B) at redshifts $z_A = 2.81099$ and $z_B = 2.81112$. The light from the main source ($\sim 98\%$ of the total flux) is intercepted by the two H $_2$ components and does not produce any residual flux in the saturated lines. The light from the additional source that passes by H $_2$ clouds is not absorbed and therefore produces a uniform residual flux in H $_2$ lines. The flux in the absorption line of two components A and B can be described as

$$F(\lambda) = (1 - f_c)F_{\text{total}} + f_cF_{\text{total}}e^{-\tau_A(\lambda)}e^{-\tau_B(\lambda)}, \quad (3)$$

where f_c (in relative units) is the covering factor for H $_2$ lines.

However, because the physical conditions in the A and B clouds (such as linear size, volume density, etc.) might be different, we can expect the covering factors of quasar emission regions by two H $_2$ clouds also to be different. In this case the construction of the H $_2$ line profiles is more complicated and we present an analysis of this case below (see Appendix A). Here, it is important to note that taking into account two covering factors does not allow for a better fit to the H $_2$ lines (see the discussion in Appendix A).

Then the absorption lines for each J level were de-

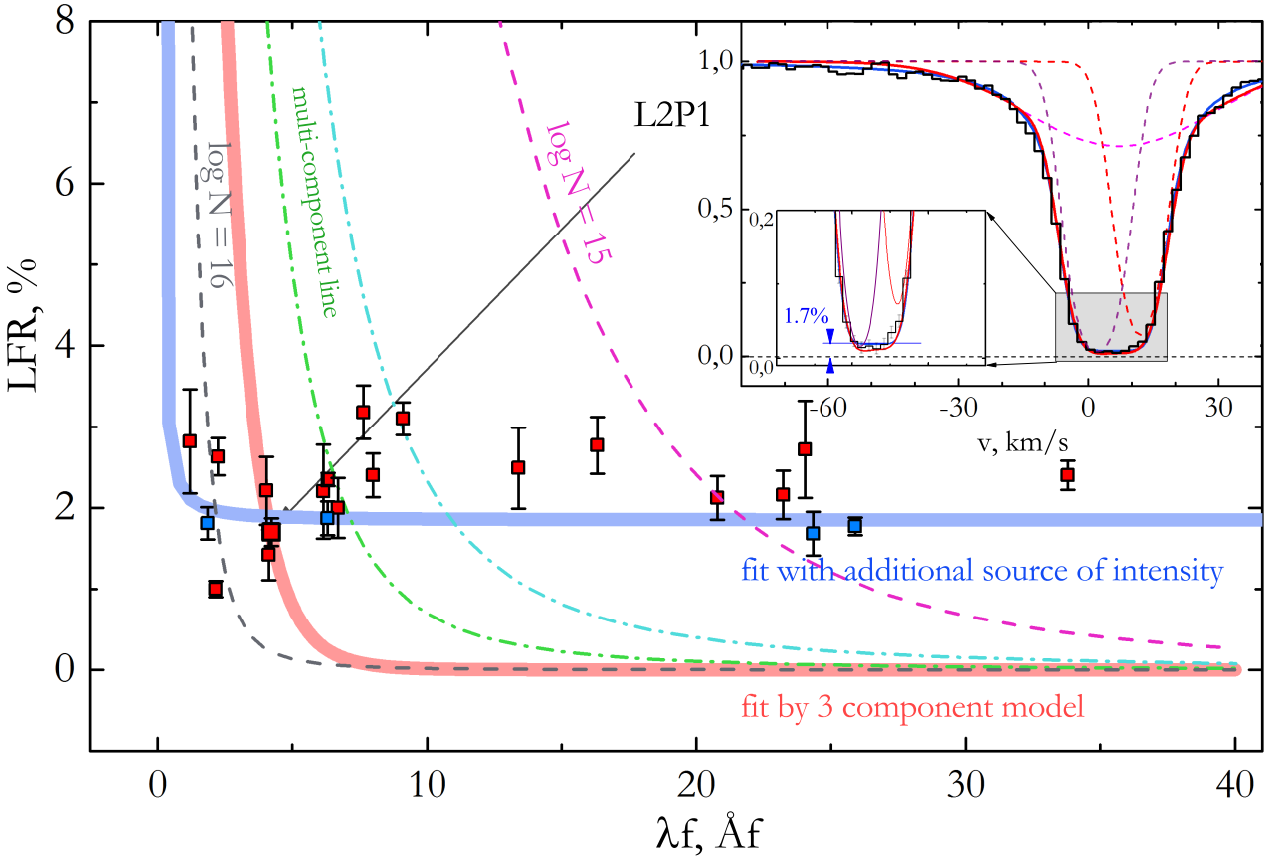


Figure 7. The residual flux at the bottom of the H₂ absorption lines is given versus the parameter λf (where f is the oscillator strength of a line). Blue and red points correspond to the H₂ lines from the $J = 0$ and $J = 1$ levels. The theoretical flux at the bottom of the one-component line with a fixed column density N and Doppler parameter b is shown by the dashed curve. The violet and grey curves correspond to column densities $\log N(H_2) = 15$ and 16. It is seen that all points cannot be described by one curve simultaneously. The blue dash-dotted line represents the calculated residual flux at the bottom of a composite line, which consists of two components with $\log N(H_2) = 15$ for both lines and a velocity separation of $\delta v = 2 \text{ km s}^{-1}$. The green dash-dotted line presents the same model for three components with the same column densities and velocity separations of $\delta v = 2$ and 4 km s^{-1} , respectively (see text). An example is shown in the right-hand top panel. We fit a certain H₂ line (L2P1) by two models: one component with the LFR (blue line) and three components (red line). Both models give adequate fit of the line. But model without the LFR cannot describe flux in all lines together, as shown by the thick red line in the graph. In contrast, all points are described by a one-component model with residual flux (see the thick blue line).

scribed using seven fitting parameters: z_A , z_B , b_A , b_B , N_A , N_B , f_c . We used uniform values of f_c over the whole wavelength range, because the residual flux in the H₂ lines is almost independent of the wavelength (see Fig. 5). The Doppler parameter b is a function of the rotational level J . To estimate fitting parameters Markov Chain Monte Carlo (MCMC) method was implemented, and to speed the convergence the Affine invariant ensemble sampler by Goodman & Weare (2010) was used. The main advantage of this searching algorithm is to better explore a parameter space and to avoid using the partial derivatives of the χ^2 function which eases a number of numerical issues. This allowed for more reliable estimates of the fitting parameters in comparison with other algorithms.

4.5 Fitting results

The H₂ absorption system at $z = 2.811$ has more than 130 absorption lines from $J = 0$ to $J = 5$ rotational levels. For

the current analysis, we selected H₂ lines that are free of any obvious blends. The sample examined contains 99 lines. The best fit of H₂ lines are shown in Fig.C1–Fig.C5 ranked following wavelength positions. The best-fitting parameters are illustrated in Table 3. The reduced χ^2 is 1.08 (the number of fitting points ~ 1500).

The H₂ absorption system is highly saturated. The total H₂ column densities are 18.10 ± 0.02 and 17.82 ± 0.02 for the A and B components consequently. This is consistent with the presence of the Lorentzian wings in the profiles of $J = 0$ and $J = 1$ levels. The obtained ortho-to-para ratios are 2.7 ± 0.1 and 3.2 ± 0.3 for the A and B components, respectively. The corresponding kinetic temperatures of the H₂ clouds are $T_{01,A} = 141 \pm 6 \text{ K}$ and $T_{01,B} = 167 \pm 13 \text{ K}$.

Fig. 8 shows a comparison of the H₂ excitation diagrams for our measurements and those of previous work. The left-hand panel shows the result of the analysis performed by King et al. (2011), the right-hand panel shows the result from the present work. Because the results presented here

Table 3. Column densities and Doppler parameters obtained from Voigt profile fitting of the H_2 system at $z_{\text{abs}} = 2.811$ towards Q 0528–250 after taking care of partial coverage.

System	J	z_{abs}	$\log N (\text{cm}^{-2})$	b (km s^{-1})
A	0	2.8109950(20)	17.50 ± 0.02	2.66 ± 0.05
	1	2.8109950(20)	17.93 ± 0.01	2.71 ± 0.05
	2	2.8109952(5)	16.87 ± 0.03	2.75 ± 0.03
	3	2.8109934(5)	15.97 ± 0.07	2.87 ± 0.07
	4	2.8109938(8)	14.18 ± 0.01	4.79 ± 0.11
	5	2.8109938(8)	13.58 ± 0.02	5.04 ± 0.39
B	0	2.8111240(20)	17.16 ± 0.03	1.17 ± 0.06
	1	2.8111230(20)	17.67 ± 0.02	1.14 ± 0.06
	2	2.8111235(7)	16.64 ± 0.03	1.22 ± 0.02
	3	2.8111238(6)	16.24 ± 0.06	1.25 ± 0.03
	4	2.8111231(6)	14.20 ± 0.01	1.72 ± 0.09
	5	2.8111231(6)	13.60 ± 0.02	2.38 ± 0.45

are close to data reported by Srianand et al. (2005), these are not shown here. We show excitation diagrams for two H_2 components at $z_A = 2.81099$ (2.811001 found by King et al. (2011)) and $z_B = 2.81112$. The third H_2 component found by King et al. (2011) at $z_C = 2.8109346(11)$ is represented by the green stars. Although the ratio of $J = 0$ and $J = 1$ levels of third component is the same as in other components, the excitation diagram is not physically realistic (the excitation temperatures T_{02} and T_{13} for the third component are negative). This might be the result of the incorrect model being used. It is seen, that the discrepancy between our results and those of King et al. (2011) is larger only for the low J levels, where the influence of the partial coverage effect on the structure of the line profiles is significant. For high J levels, where column densities of H_2 are less, the results agree in 1σ . To sum up, the total column density of H_2 from the measurement is 18.284 ± 0.025 , that is about two orders of magnitude larger than the value reported by King et al. (2011) 16.556 ± 0.024 .

It should be noted, that the same values of N and b parameters for all transitions of one J level were used. Using the model with taking into account the partial coverage effect we obtain the reduced $\chi^2 \simeq 1$ without an increase of the statistical errors of the spectrum. This is important, because in the previous analysis of H_2 system in Q 0528–250 King et al. (2011) noted that without artificially increasing the statistical errors, the reduced χ^2 was $\gg 1$ (see the caption of table 6 in King et al. 2011).

The value of the residual flux in H_2 lines is fitted as an independent parameter of an analysis. The best value is $2.40 \pm 0.07\%$ of the continuum, which agrees with the average value of the residual flux obtained from the analysis of $J = 0, 1$ H_2 lines (see Section 4.3).

5 HD MOLECULES

In the new spectrum (obtained by co-adding all previous and additional new observations) the molecular HD lines associated with the H_2 absorption system were detected (us-

Table 4. Best fitting parameters for HD molecular lines in the spectrum of Q 0528–250.

z_{abs}	$\log N (\text{cm}^{-2})$	b (km s^{-1})
2.811121 ± 0.000002	13.33 ± 0.02	2.25 ± 0.53
HD/2 H_2	$(1.48 \pm 0.10) \times 10^{-5}$	

ing improved laboratory wavelengths, Ivanov et al. 2010). The presence of HD lines in this system was first reported by King et al. (2011). The HD molecular lines are present only in the component B. Some of the HD lines are shown in Fig. 9. We have estimated the HD column density $\log N(\text{HD})_B = 13.33 \pm 0.02$ by analysis of the two most prominent unblended absorption lines, L4-0R(0) and L8-0R(0). The results of Voigt profile fitting are presented in Table 4. Other HD lines are highly blended and cannot be used in the analysis. The obtained column density is significantly less than that required to produce self-shielding, $\log N(\text{HD}) \simeq 15$, thus we can set only a lower limit to the isotopic ratio D/H in the cloud. Because the total column density of H_2 in the component B is $\log N(H_2) = 17.85 \pm 0.02$, we estimate $D/H \geq N(\text{HD})/2N(H_2) = (1.48 \pm 0.10) \times 10^{-5}$. The obtained HD column density is close to the result, $\log N(\text{HD}) = 13.267 \pm 0.072$, reported by King et al. (2011). However, taking into account the significantly larger H_2 column density of the component B we have obtained a lower value of $N(\text{HD})/2N(H_2)$ than the result by King et al. (2011). This limit is consistent with D/H ratio obtained from the analyses of atomic species in quasar spectra (e.g. Olive et al. 2012). The comparison of this result with other $N(\text{HD})/2N(H_2)$ measurements at high redshift is shown in Fig. 10. The $N(\text{HD})/2N(H_2)$ in this system is consistent with other values and correspond to predictions of deuterium chemistry models of diffuse ISM clouds (e.g. Balashev et al. 2010; Liszt 2014).

Note that in the component B we detect HD and C₁ whereas in the component A these species are not present, despite the higher H_2 column density of this component in comparison with the component B. As for the component A we set an upper limit for HD and C₁ column densities which are $\log N(\text{HD})_A \leq 13.1$ and $\log N(\text{C}_1)_A \leq 12.0$. The lack of HD and C₁ in the component A might be the result of higher local UV radiation (e.g. bright young stars near cloud A). It can destroy HD and ionize C₁ while the H_2 molecules self-shield against the local stellar radiation because to their high column density.

6 DISCUSSION

The presence of a residual flux at the bottom of the saturated lines of the H_2 system at $z_{\text{abs}} = 2.811$ towards Q 0528–250 can be interpreted according to the arguments described in the following subsections.

6.1 Unresolved multicomponent quasars

At redshift $z \sim 2$, the internal structures in the emitting regions of quasars with transverse dimensions $\lesssim 3 \text{ kpc}$

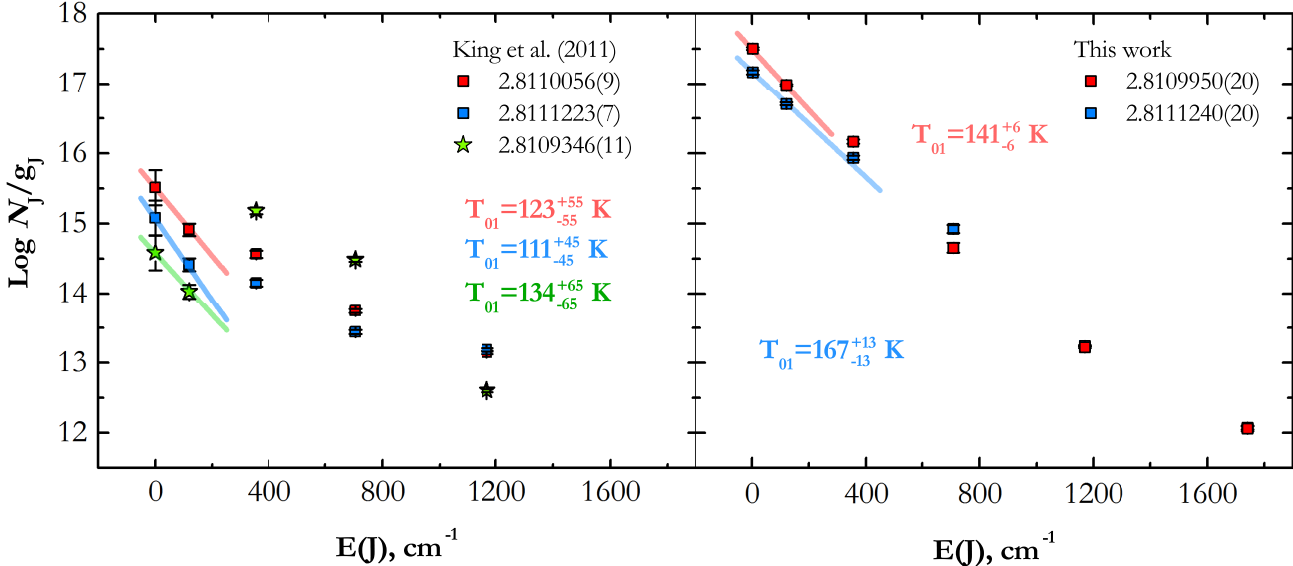


Figure 8. The excitation diagram for H_2 towards Q 0528–250. Here, N_J is the column density of the transition from the J level with g_J degeneracy. Solid lines (blue, red and green) correspond to the excitation temperature T_{01} derived from $J = 0$ and $J = 1$ levels. The left-hand panel shows the result of the analysis performed by King et al. (2011). The excitation diagrams for different components of the H_2 system are shown by blue, red and green colors. The right-hand panel shows the results from our present work. Instead of three unsaturated components we use two components with higher H_2 column densities.

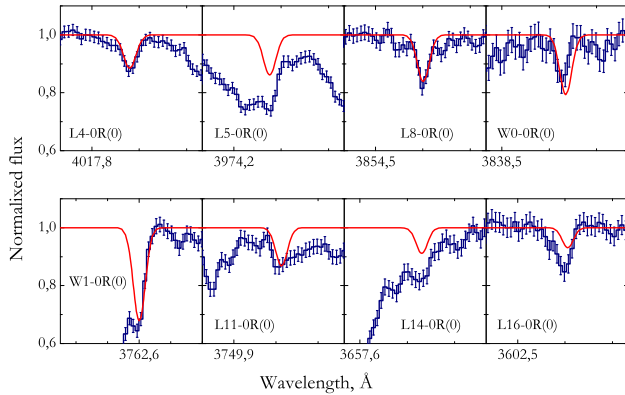


Figure 9. The line profiles of HD molecules in the absorption system at $z_{\text{abs}} = 2.811$ in the spectrum of Q 0528–250. HD lines are detected in component B only. The fit to the W0-0R(0) line is inconsistent owing to a poor definition of the local continuum near the base of the Ly α line of the second DLA system at $z_{\text{abs}} = 2.14$.

are unresolved by UVES observations. For example, binary quasars with separations of the order of ~ 10 kpc (Hennawi et al. 2006; Vivek et al. 2009) might remain unresolved. Partial coverage can arise if Q 0528–250 has a complex multicomponent structure and if not all of the components are covered by the absorbing H_2 clouds.

The available Very Long Baseline Array (VLBA) image of Q 0528–250 (Kanekar et al. 2009; Srianand et al. 2012) shows an unresolved component containing ~ 94 per cent of the total flux in the radio band (see table 6 of Srianand et al. 2012). Another ~ 6 per cent is probably emitted by a diffuse component. However, it is intriguing to note the consistency of these numbers with our findings. The spatial size of ra-

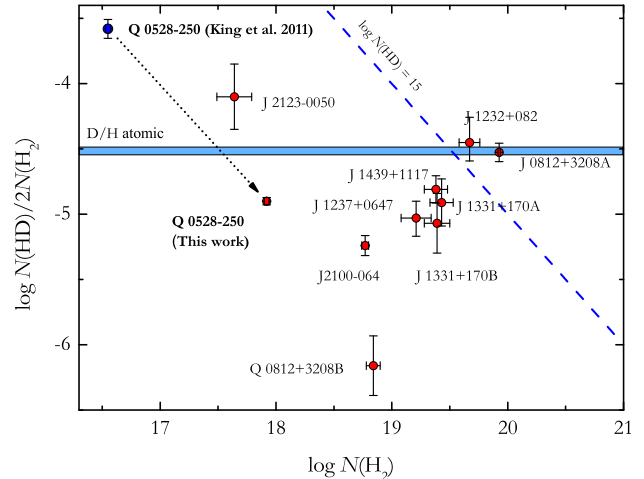


Figure 10. The measurements of $N(\text{HD})/N(\text{H}_2)$ vs $\log N(\text{H}_2)$ in absorption systems at high redshift. The data are taken from Ivanchik et al. (2015). The estimates of $N(\text{HD})/N(\text{H}_2)$ toward Q 0528–250 from this work and King et al. (2011) are shown by red and blue circles, accordingly. The blue horizontal strip represents the ratio of atomic D1 and H1 measured in quasar spectra (Olive et al. 2012). The solid dashed line corresponds to constant column density of HD, $\log N(\text{HD}) = 15$.

dio emission core component is 65×380 pc (Kanekar et al. 2009), that is significantly larger than the size of the H_2 clouds. We have also looked at the images of PKS 0528–250 in 13 and 4 cm taken as part of National Radio Astronomy Observatory's VLBA calibrators. The sources are unresolved even at higher resolution achieved in these images.

6.2 Dust scattering

Scattering by dust is characterized by a narrow radiation pattern. About 90 per cent of the total flux is scattered towards the observer within less than 5-deg opening angle (e.g. Draine 2003). The size of the scattering region can be much larger than the size of an H_2 cloud. This is why, even in the case of total coverage of the QSO by an H_2 cloud, the scattered radiation can be registered as a residual flux in the bottom of H_2 lines. The scattered flux by a dust-rich region of a DLA system can be estimated as

$$F_{sc} = F (1 - e^{-\tau_{DLA}}) \frac{\Omega_{QSO}^* \Omega_{DLA}}{\Omega_{sc}}, \quad (4)$$

where F is the flux that passes through an H_2 cloud and is registered by the observer, τ_{DLA} is the mean optical depth along the line of sight toward the quasar, Ω_{QSO} and Ω_{DLA} are the solid angles (measured by an observer on Earth) of the QSO emission region and the scattering region, accordingly. Ω_{QSO}^* is the solid angle of the QSO emission region measured by an observer at the position of the DLA and Ω_{sc} is the solid angle in which most of radiation is scattered by dust. Therefore, the residual flux in the bottom of H_2 lines is $LFR = F_{sc}/F$. Assuming that a typical dimension of the scattering region is as large as 1–10 kpc, LFR can be of the order of several percent. This is consistent with observations. The scattered radiation can produce a non-zero residual flux for metal lines also. However, this is not detected for Q 0528–250.

6.3 Jet-cloud interaction

The jet emission pointing toward us contributes to the continuum in the optical band. The extended part of the jet interacts with the external ISM and can warm up a cloud which is distant from the central source. Similar situation has been detected in the deep radio-optical-X-ray observations of the radio galaxy PKS B2152–699 by (Worrall et al. 2012), who have reported the first high-resolution observations of the radio jet in the direction of an optical emission-line high ionization cloud. The *Hubble Space Telescope* image shows not only emission in the region of the high-ionized cloud – interpreted as ionized gas by Tadhunter et al. (1988) and Fosbury et al. (1998) – but also emission associated with a radio knot. The measured optical flux density of this knot at 4.97×10^{14} Hz is $2.5 \pm 0.2 \mu\text{Jy}$ (Worrall et al. 2012). This is strikingly similar to the value of the residual flux in the V optical band which is $2.4 \pm 0.1 \mu\text{Jy}$ (using the apparent magnitude $m_V = 17.34$ of Q 0528–250, Véron-Cetty & Véron (2010)). The variability of a jet emission (during from a few days up to a month) should be high and should also induce variability of the residual flux in the H_2 line. This could be tested by further observations.

7 CONCLUSION

We have performed a detailed analysis of the H_2 system at $z_{abs} = 2.811$ towards the quasar Q 0528–250. This is a well-known system and the first detection of H_2 molecules at high redshift (Levshakov & Varshalovich 1985). The system has been analysed in a variety of research, but the results

obtained are not consistent (see Table 2). The discrepancies can be explained by the presence of a residual flux in the bottom of H_2 lines, which has not been considered in previous research. We have derived the mean value of the residual flux as (2.22 ± 0.54) per cent of the continuum. This is significantly higher than the zero flux level, (-0.21 ± 0.22) per cent, determined by analysis of the Ly α forest lines.

Taking into account the residual flux in the H_2 lines we have obtained a consistent fit of the H_2 system using a two-component model with high column densities. The derived total column densities of components A and B are $\log N(H_2) = 18.10 \pm 0.02$ and 17.82 ± 0.02 , respectively.

We have performed the analysis of HD absorption lines detected only in component B. The estimated column density is $\log N(HD) = 13.33 \pm 0.02$ and thus we derive $N(HD)/2N(H_2) = (1.48 \pm 0.13) \times 10^{-5}$. This value is consistent with other measurements of $N(HD)/2N(H_2)$ in quasar spectra at high redshift and can be considered as a lower limit of the primordial deuterium abundance (Balashev et al. 2010).

Some interpretations for the presence of the residual flux are being offered here: (i) a multicomponent quasar; (ii) scattering by dust; (iii) a jet-cloud interaction. We favour the latter interpretation (iii). However, new optical and radio observations of Q 0528–250 are necessary to confirm this and reject the others.

We argue that taking into account partial coverage effects is crucial for any analysis of H_2 bearing absorption systems in particular when studying the physical state of high-redshift ISM.

Acknowledgments. This work is based on observations carried out at the European Southern Observatory (ESO) under programmes ID 66.A-0594(A) (PI: Molaro), ID 68.A-0600(A) (PI: Ledoux), ID 68.A-0106(A) (PI: Petitjean) and ID 082.A-0087(A) (PI: Ubachs) with the UVES spectrograph installed at the Kueyen UT2 on Cerro Paranal, Chile.

The work is supported by Dynasty foundation and by the RF President Programme(grant MK-4861.2013.2). RS and PPJ gratefully acknowledge support from the Indo-French Centre for the Promotion of Advanced Research (IFCPAR) under Project N.4304-2.

REFERENCES

- Abdo A. A. et al., 2010, *Nature*, 463, 919
- Albornoz Vásquez D., Rahmani H., Noterdaeme P., Petitjean P., Srianand R., Ledoux C., 2014, *Astron. & Astrophys.*, 562, A88
- Balashev S. A., Ivanchik A. V., Varshalovich D. A., 2010, *Astronomy Letters*, 36, 761
- Balashev S. A., Petitjean P., Ivanchik A. V., Ledoux C., Srianand R., Noterdaeme P., Varshalovich D. A., 2011, *Mon. Not. of Royal Astron. Soc.*, 418, 357
- Blackburne J. A., Pooley D., Rappaport S., Schechter P. L., 2011, *Astrophys. Journal*, 729, 34
- Chelouche D., Daniel E., 2012, *Astrophys. Journal*, 747, 62
- Ćirković M. M., Damjanov I., Lalović A., 2006, *Baltic Astronomy*, 15, 571
- Cowie L. L., Songaila A., 1995, *Astrophys. Journal*, 453, 596

Dekker H., D'Odorico S., Kaufer A., Delabre B., Kotzlowski H., 2000, in Society of Photo-Optical Instrumentation Engineers (SPIE) Conference Series, Vol. 4008, Optical and IR Telescope Instrumentation and Detectors, Iye M., Moorwood A. F., eds., pp. 534–545

Draine B. T., 2003, *Astrophys. Journal*, 598, 1017

Foltz C. B., Chaffee, Jr. F. H., Black J. H., 1988, *Astrophys. Journal*, 324, 267

Fosbury R. A. E., Morganti R., Wilson W., Ekers R. D., di Serego Alighieri S., Tadhunter C. N., 1998, *Mon. Not. of Royal Astron. Soc.*, 296, 701

Goodman J., Weare J., 2010, *Comm. App. Math. and Comp. Sci.*, 5, 65

Hamann F. W., Kanekar N., Prochaska J., Murphy M. T., Milutinovic N., Ellison S., Ubachs W., 2010, in *Bulletin of the American Astronomical Society*, Vol. 41, American Astronomical Society Meeting Abstracts #216, p. 420.03

Hennawi J. F. et al., 2006, *Astronomical Journal*, 131, 1

Ivanchik A. V., Balashev S. A., Varshalovich D. A., Klimenko V. V., 2015, *Astronomy Reports*, 59, 100

Ivanchik A. V., Petitjean P., Balashev S. A., Srianand R., Varshalovich D. A., Ledoux C., Noterdaeme P., 2010, *Mon. Not. of Royal Astron. Soc.*, 404, 1583

Ivanov T. I., Dickenson G. D., Roudjane M., de Olivera N., Joyeux D., Nahon L., Tchang-Brillet W.-Ü. L., Ubachs W., 2010, *Molecular Physics*, 104, 771

Jaffe W. et al., 2004, *Nature*, 429, 47

Jiménez-Vicente J., Mediavilla E., Muñoz J. A., Kochanek C. S., 2012, *Astrophys. Journal*, 751, 106

Jones T. M., Misawa T., Charlton J. C., Mshar A. C., Ferland G. J., 2010, *Astrophys. Journal*, 715, 1497

Kanekar N., Lane W. M., Momjian E., Briggs F. H., Chennalur J. N., 2009, *Mon. Not. of Royal Astron. Soc.*, 394, L61

Kaspi S., Brandt W. N., Maoz D., Netzer H., Schneider D. P., Shemmer O., 2007, *Astrophys. Journal*, 659, 997

King J. A., Murphy M. T., Ubachs W., Webb J. K., 2011, *Mon. Not. of Royal Astron. Soc.*, 417, 3010

Levshakov S. A., Varshalovich D. A., 1985, *Mon. Not. of Royal Astron. Soc.*, 212, 517

Liszt H. S., 2014, *ArXiv e-prints*

López-Gonzaga N., Jaffe W., Burtscher L., Tristram K. R. W., Meisenheimer K., 2014, *Astron. & Astrophys.*, 565, A71

Muzahid S., Srianand R., Arav N., Savage B. D., Narayanan A., 2013, *Mon. Not. of Royal Astron. Soc.*, 431, 2885

Noterdaeme P., Ledoux C., Petitjean P., Srianand R., 2008, *Astron. & Astrophys.*, 481, 327

Noterdaeme P., Petitjean P., Srianand R., Ledoux C., Le Petit F., 2007, *Astron. & Astrophys.*, 469, 425

Noterdaeme P., Petitjean P., Srianand R., Ledoux C., López S., 2011, *Astron. & Astrophys.*, 526, L7

Olive K. A., Petitjean P., Vangioni E., Silk J., 2012, *Mon. Not. of Royal Astron. Soc.*, 426, 1427

Petitjean P., Aracil B., Srianand R., Ibata R., 2000, *Astron. & Astrophys.*, 359, 457

Petitjean P., Rauch M., Carswell R. F., 1994, *Astron. & Astrophys.*, 291, 29

Potekhin A. Y., Ivanchik A. V., Varshalovich D. A., Lanzetta K. M., Baldwin J. A., Williger G. M., Carswell R. F., 1998, *Astrophys. Journal*, 505, 523

Rahmani H. et al., 2013, *Mon. Not. of Royal Astron. Soc.*, 435, 861

Rupke D. S., Veilleux S., Sanders D. B., 2005, *Astrophys. Journal Suppl. Ser.*, 160, 87

Sluse D. et al., 2011, *Astron. & Astrophys.*, 528, A100

Srianand R., Gupta N., Petitjean P., Noterdaeme P., Ledoux C., Salter C. J., Saikia D. J., 2012, *Mon. Not. of Royal Astron. Soc.*, 421, 651

Srianand R., Petitjean P., 1998, *Astron. & Astrophys.*, 335, 33

Srianand R., Petitjean P., Ledoux C., 2000, *Nature*, 408, 931

Srianand R., Petitjean P., Ledoux C., Ferland G., Shaw G., 2005, *Mon. Not. of Royal Astron. Soc.*, 362, 549

Sugiura N., 1978, *Commun. Stat. A-Theor.*, 7, 13

Tadhunter C. N., Fosbury R. A. E., di Serego Alighieri S., Bland J., Danziger I. J., Goss W. M., McAdam W. B., Snijders M. A. J., 1988, *Mon. Not. of Royal Astron. Soc.*, 235, 403

Tristram K. R. W., Burtscher L., Jaffe W., Meisenheimer K., Hönig S. F., Kishimoto M., Schartmann M., Weigelt G., 2014, *Astron. & Astrophys.*, 563, A82

Ubachs W., Reinhold E., 2004, *Physical Review Letters*, 92, 101302

Vanden Berk D. E. et al., 2001, *Astronomical Journal*, 122, 549

Varshalovich D. A., Ivanchik A. V., Petitjean P., Srianand R., Ledoux C., 2001, *Astronomy Letters*, 27, 683

Varshalovich D. A., Levshakov S. A., 1993, *Soviet Journal of Experimental and Theoretical Physics Letters*, 58, 237

Véron-Cetty M.-P., Véron P., 2010, *Astron. & Astrophys.*, 518, A10

Vivek M., Srianand R., Noterdaeme P., Mohan V., Kuriakose V. C., 2009, *Mon. Not. of Royal Astron. Soc.*, 400, L6

Whitmore J. B., Murphy M. T., Griest K., 2010, *Astrophys. Journal*, 723, 89

Worrall D. M., Birkinshaw M., Young A. J., Momtahan K., Fosbury R. A. E., Morganti R., Tadhunter C. N., Verdoes Kleijn G., 2012, *Mon. Not. of Royal Astron. Soc.*, 424, 1346

APPENDIX A: TEST OF A MODEL WITH TWO ADDITIONAL SOURCES OF RESIDUAL FLUX

In this section, we consider a model of absorption system, where the projected area over the illuminating source is different for components A and B. In that case a structure of H_2 line profiles is more complicated. To describe a flux detected by an observer, we divide a quasar emission region into three parts: the main source and two additional sources. The main source is covered by both H_2 clouds and does not produce the residual flux in absorption lines. Additional sources can produce the residual flux in two different ways (depending on the geometry of additional sources and H_2 clouds, see Fig. A1) as follows.

(i) One source (not covered by both clouds) produces the same residual flux in profiles of both H_2 systems. Another source is covered by one cloud and produces residual

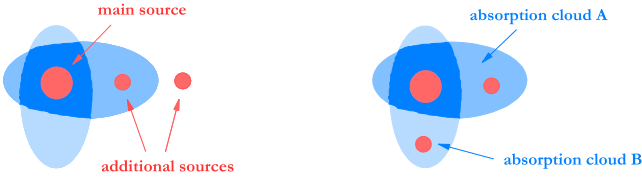


Figure A1. An illustration of the possible explanation of the partial coverage effect for a case with independent sources of radiation (see text for detail).

Table A1. A Comparison between models of the H_2 system with a different number of additional sources of radiation. *A* indicates the model with one additional source (which used in this work). *B* and *C* correspond to models (i) and (ii) described in see App. A. *p* given the number of fitting parameters, AICC is the Akaike information criterion (see Sect. 4.1). *m* and *n* indicate the intensity of additional sources relative to the total flux of a quasar.

Model	<i>p</i>	AICC	ΔAICC	<i>m</i> , 10^{-2}	<i>n</i> , 10^{-2}
A	31	3096.0	12.9	2.4 ± 0.1	0
B	32	3083.1	0	2.0 ± 0.1	4.0 ± 0.3
C	32	3331.1	248.0	2.4 ± 0.1	7.6 ± 0.3

flux only in profile of the second system:

$$F(\lambda) = mF_{total}(\lambda) + nF_{total}(\lambda)e^{-\tau_A(\lambda)} + (1 - m - n)F_{total}(\lambda)e^{-\tau_A(\lambda) - \tau_B(\lambda)}. \quad (\text{A1})$$

(ii) Each source produces the residual flux only for one system:

$$F(\lambda) = mF_{total}(\lambda)e^{-\tau_B(\lambda)} + nF_{total}(\lambda)e^{-\tau_A(\lambda)} + (1 - m - n)F_{total}(\lambda)e^{-\tau_A(\lambda) - \tau_B(\lambda)}, \quad (\text{A2})$$

where *m* and *n* indicate intensities of additional sources in relative units. The results of Voigt profile fitting of H_2 lines using different models of the H_2 system are presented in Table A1. The values of AICC for models *A* and *B* are significantly lower than for model *C*, which could indicate the presence of one additional source of quasar radiation which uncovered by both H_2 clouds. Taking into account the second additional source (for system B) does not dramatically changed the AICC value and we have not found strong evidence for choosing a preferred model. Therefore, we use the simplest model (with one additional source) to analyse the H_2 system.

APPENDIX B: THE EXPOSURE SHIFT ANALYSIS

Because the final spectrum of Q 0528–250 is the co-addition of 27 exposures the non-zero residual flux at the bottom of saturated absorption lines (such as H_2 lines) could arise due to the average velocity shifts between exposures, up to 500 m s^{-1} , and/or intra-order velocity distortions, up to 1500 m s^{-1} (e.g. Whitmore et al. 2010; Rahmani et al. 2013). Also, such a small LFR could be the result of the dramatic shift of even one exposure (e.g. Rahmani et al. 2013). In that case, all narrow saturated absorption lines would

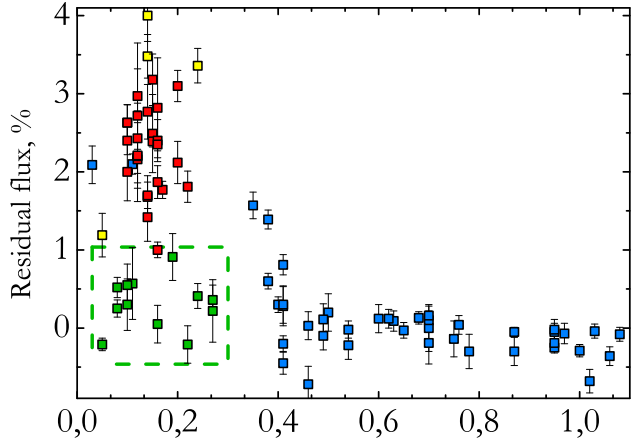


Figure B1. The dependence of residual fluxes in the bottom of lines on the widths of the bottom of lines. Blue points correspond to all saturated Ly α forest lines with $\lambda > 3500 \text{ \AA}$ and reached the zero-flux level within 5%. The yellow points mark Ly α absorbers which have also Ly β absorption lines in the spectrum. The red points represent the residual fluxes in H_2 lines. Among the Ly α forest lines there are lines with LFR < 1% and the width of the bottom < 0.3 \AA . We marked them by green colour. Existence of such lines indicate that the residual fluxes in H_2 lines are not the instrumental effect (see text for detail).

have the same non-zero residual fluxes, whereas the wide saturated absorption lines (like most of the Ly α forest lines) will go to zero. Fig. B1 shows the residual fluxes obtained in absorption lines that have the residual flux within 5 per cent of the continuum and located in the region 3500 – 4700 \AA in comparison to their widths at the bottom. The measurement procedure was described in Section 4.2. The red filled squares correspond to H_2 lines, and the blue, green and yellow filled squares correspond to the Ly α forest lines. The points marked in green represent the sample of the narrow saturated Ly α forest lines which look like the H_2 lines, but the residual flux at the bottom of the lines goes to zero. The profiles of these lines are shown in Fig. B2. The existence of such lines in the spectrum of Q 0528–250 implies that the dramatic shift between exposures does not exist, otherwise the residual flux would be present in these lines too. There are also several Ly α forest lines that have non-zero residual fluxes comparable or even larger than the average H_2 residual flux. By performing visual inspections of these lines, Ly β absorption lines for four of them (yellow squares in Fig. B1) were found, due to the fact that corresponding Ly α lines have redshifts large than 2.43. For systems with *z* lower than 2.43 the Ly β absorption lines are located in the Lyman-break region in the spectrum. The Fig. B3 shows the result of Voigt fitting analysis of these lines. All of them have small HI column densities ($\log N < 14.3$) and large Doppler parameters ($b > 25 \text{ km s}^{-1}$).

APPENDIX C: THE BEST FIT OF H_2 LINES

Here we present the figures of the best fit of the H_2 lines.

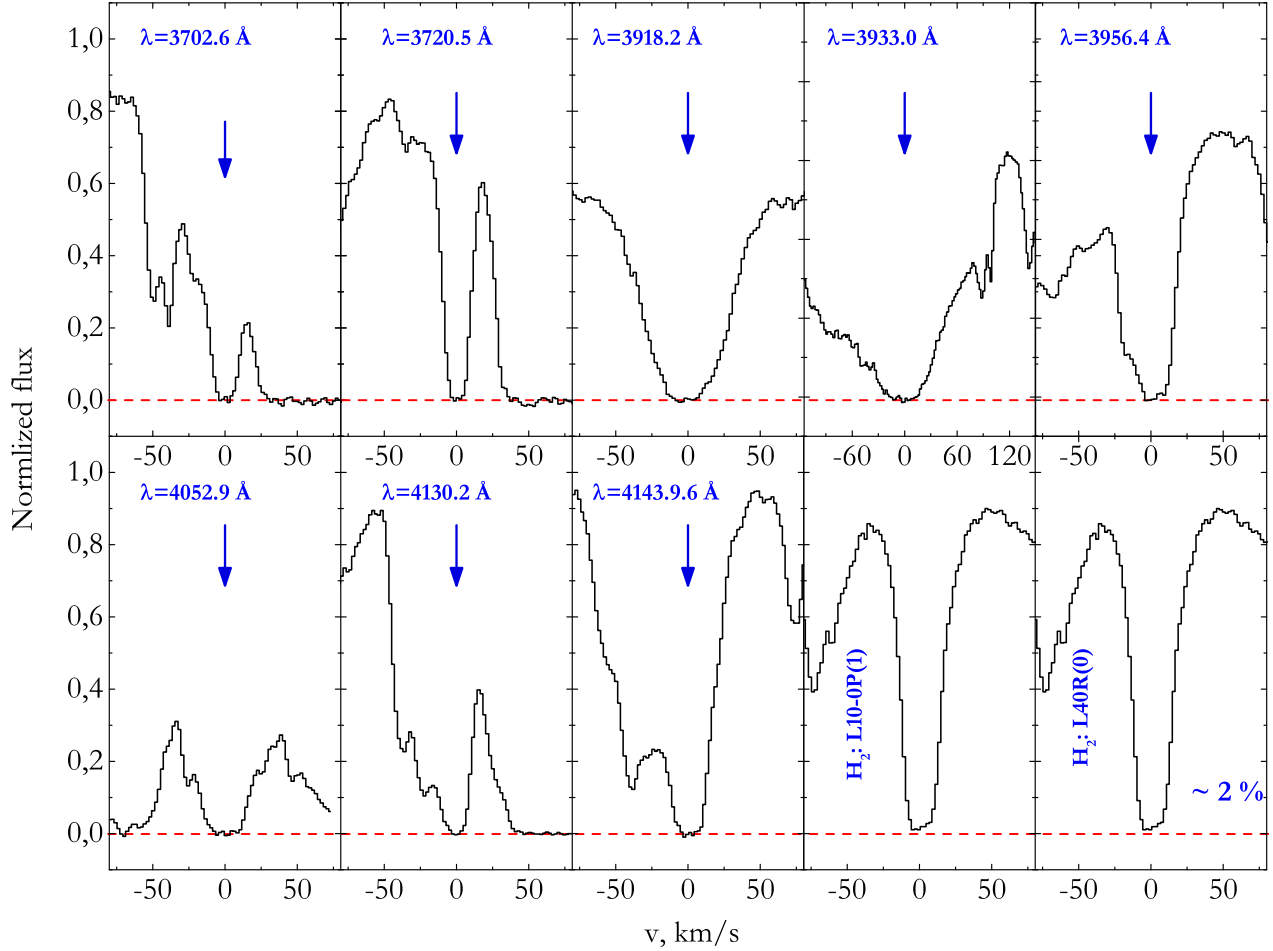


Figure B2. The profiles of the Ly α forest lines corresponded to green filled squares in Fig. B1. For comparison we show also two H $_2$ lines, L10-0P(1) and L40R(0), in the two bottom right panels. The red horizontal line represents the zero flux level.

This paper has been typeset from a \TeX / \LaTeX file prepared by the author.

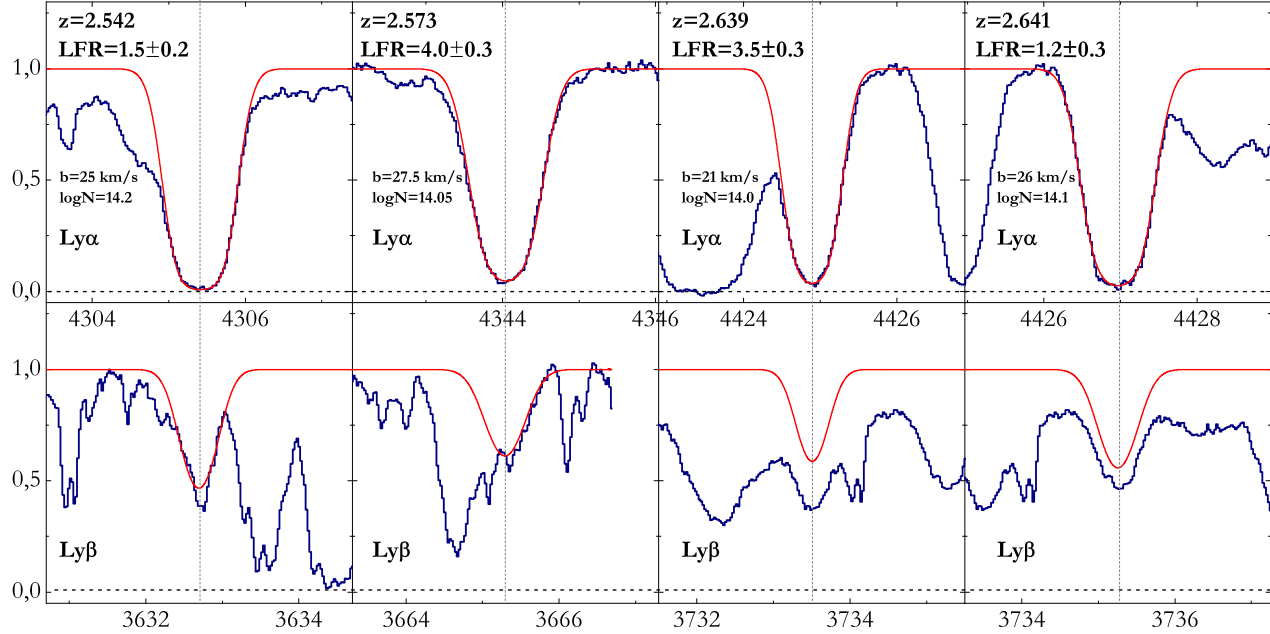


Figure B3. The profiles of the Ly α forest lines corresponded to yellow filled squares in Fig. B1. The top panels show Ly α absorptions. The bottom panels show corresponded Ly β absorptions. The best Voigt profile fit is shown by red lines.

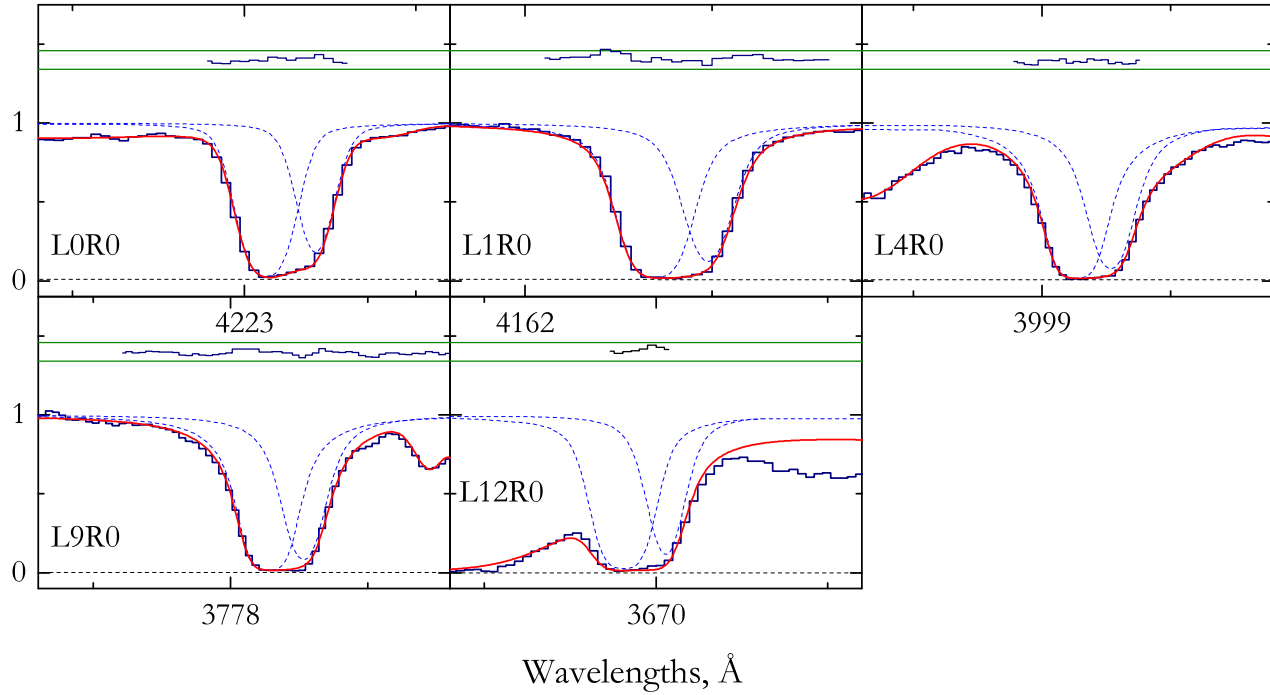


Figure C1. The best fit of the H_2 absorption lines from $J = 0$ level at $z_{\text{abs}} = 2.811$ toward Q 0528–250 (after incorporating the correction for partial coverage). Two components of absorption system are shown by blue dashed lines. The residuals between fit and data are shown in the top of each panel by dark blue line. Horizontal green lines represent $\pm 3\sigma$ levels.

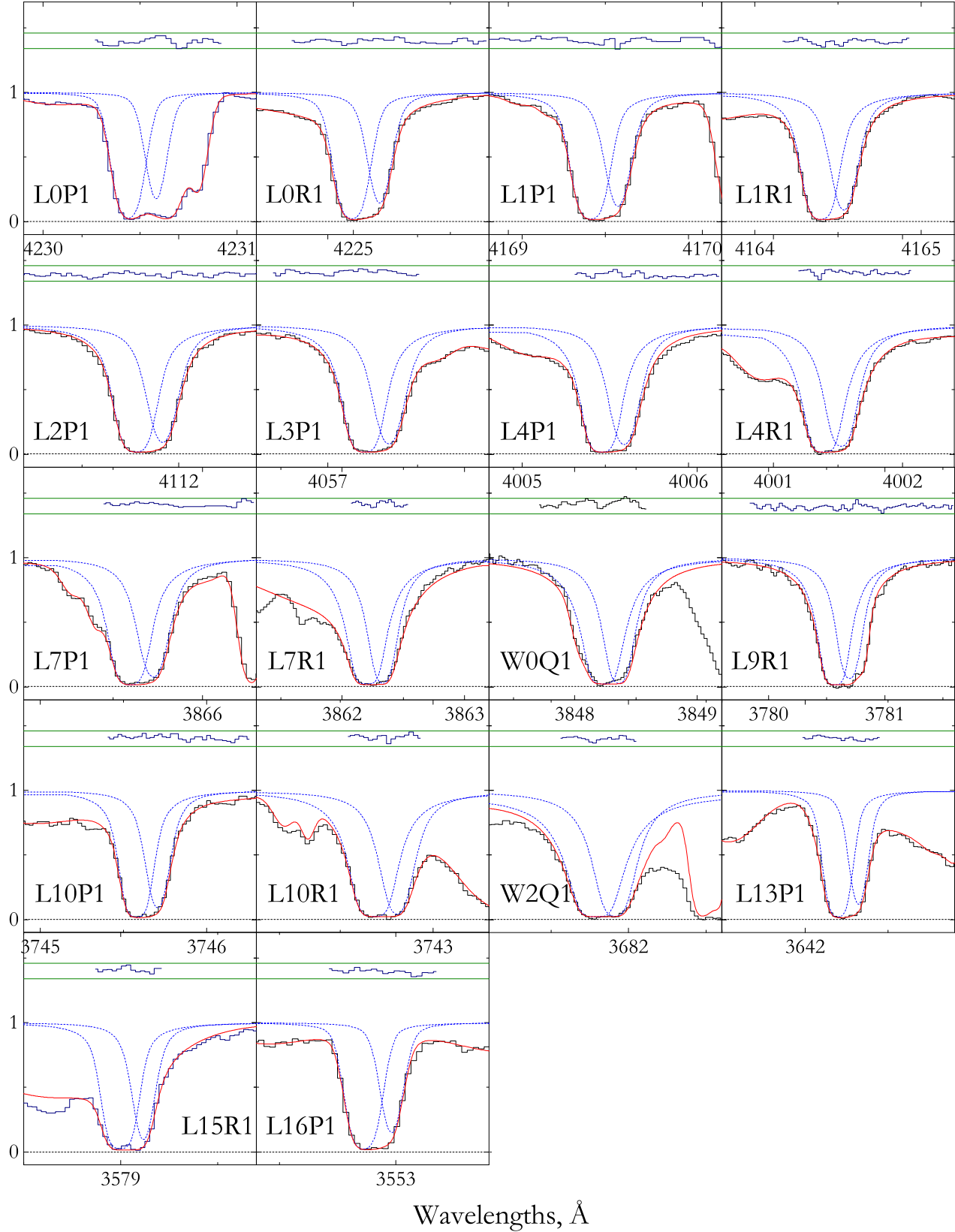


Figure C2. The best fit of the H_2 absorption lines from $J = 1$ level at $z_{\text{abs}} = 2.811$ toward Q 0528–250. Colors and lines are the same as in Figure C1.

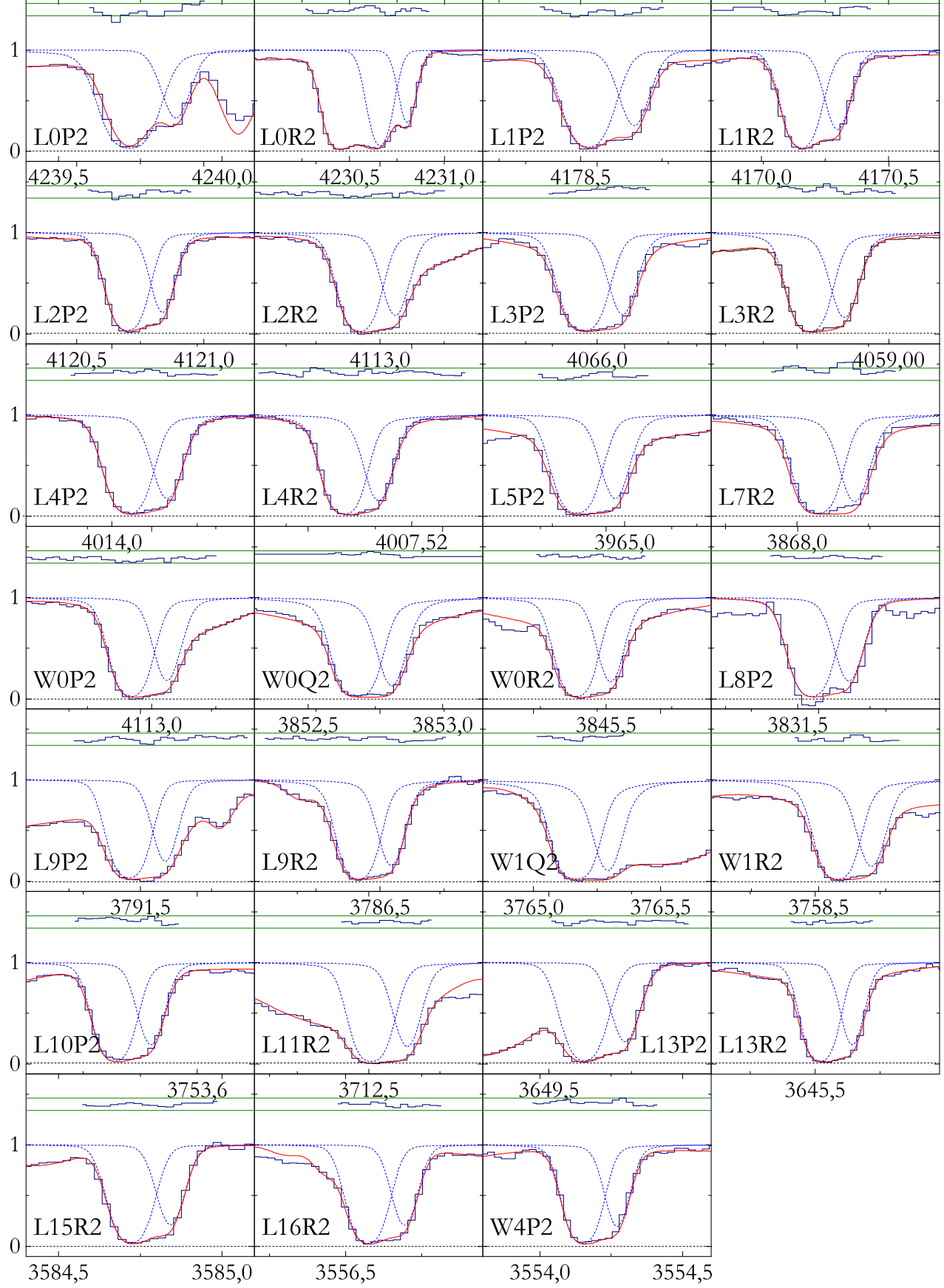


Figure C3. The best fit of the H_2 absorption lines from $J = 2$ level at $z_{\text{abs}} = 2.811$ toward Q 0528–250. Colors and lines are the same as in Figure C1.

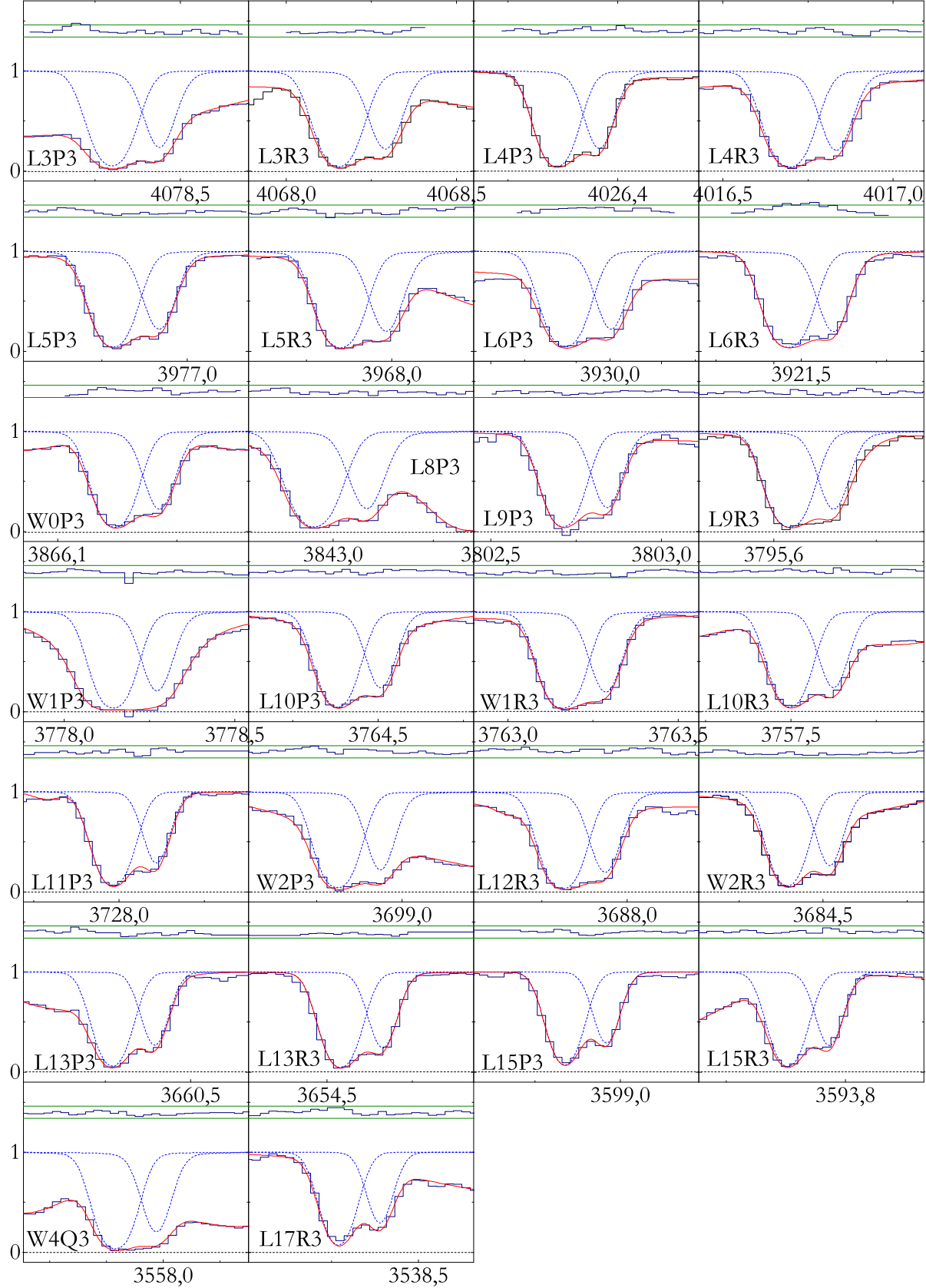


Figure C4. The best fit of the H_2 absorption lines from $J = 3$ level at $z_{\text{abs}} = 2.811$ toward Q 0528–250. Colors and lines are the same as in Figure C1.

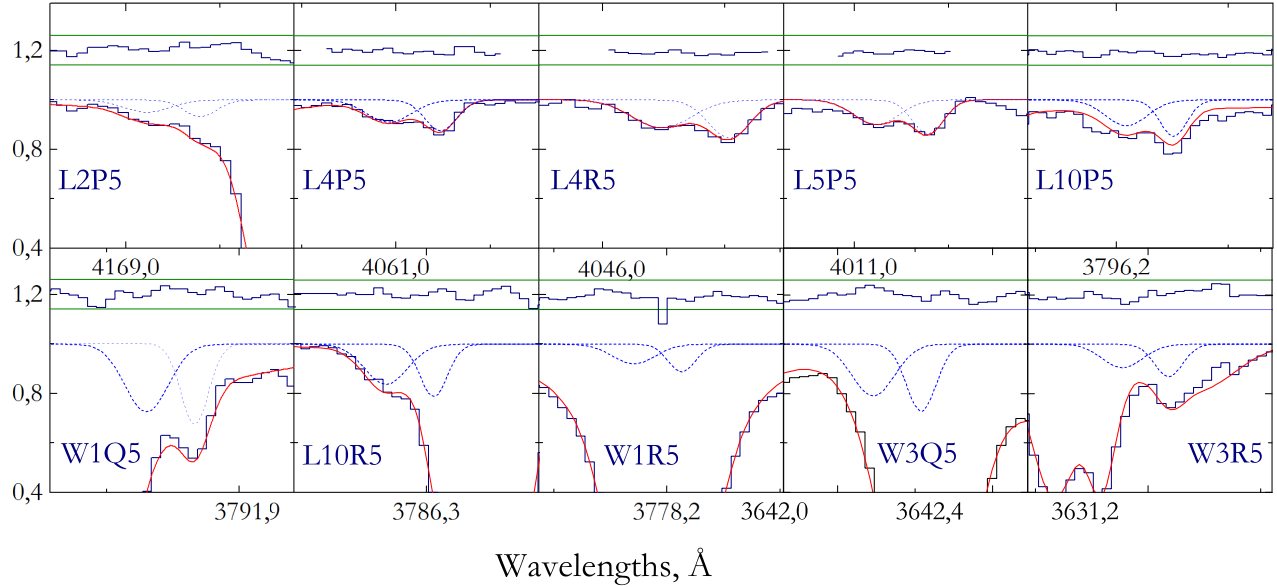


Figure C5. The best fit of the H_2 absorption lines from $J = 5$ level at $z_{\text{abs}} = 2.811$ toward Q 0528–250. Colors and lines are the same as in Figure C1.

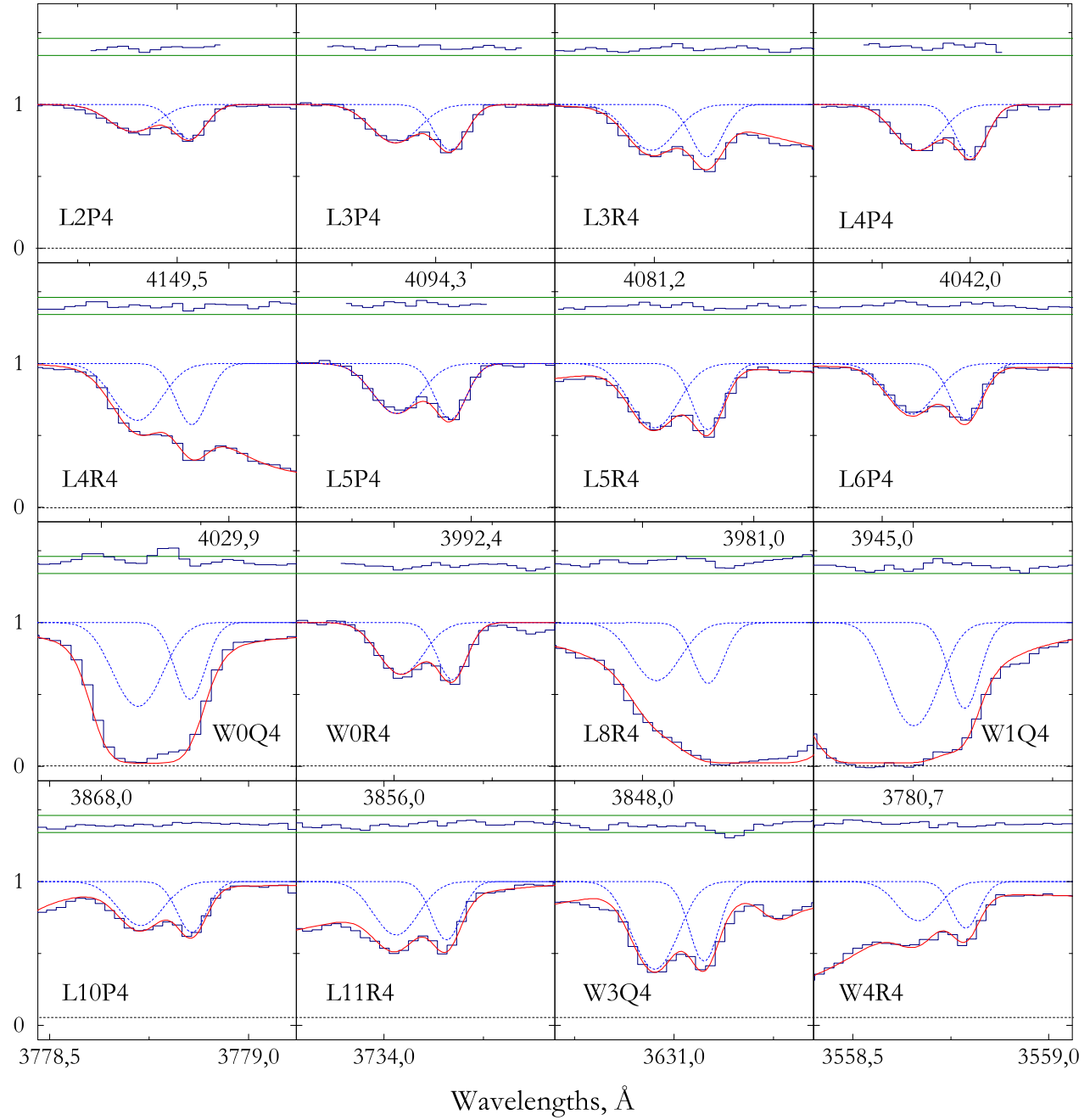


Figure C6. The best fit of the H_2 absorption lines from $J = 4$ level at $z_{\text{abs}} = 2.811$ toward Q 0528–250. Colors and lines are the same as in Figure C1.